ELSEVIER

Contents lists available at ScienceDirect

International Journal of Coal Geology

journal homepage: www.elsevier.com/locate/coal



Organic matter content and its role in shale porosity development with maturity: Insights from Baltic Basin Silurian shales

Grzegorz P. Lis a,*, Tomasz Topór b, Maria Mastalerz c

- ^a Institute of Geological Sciences, University of Wrocław, Poland
- ^b Oil and Gas Institute-National Research Institute, Cracow, Poland
- ^c Indiana Geological and Water Survey, Indiana University, Bloomington, IN, USA

ARTICLE INFO

Keywords: Porosity Organic matter Gas shale Baltic Basin Thermal maturity

ABSTRACT

Porosity, pore size distribution, and surface area are the main petrophysical characteristics indicative of gas storage capacity in shales. This paper investigates the influence of organic matter (OM) content on the evolution of these parameters at different stages of thermal maturity. Ninety-six samples of Silurian shales from the Baltic Basin ranging in maturity from immature to overmature were selected for this study. Porosity evolution was evaluated using N₂ and CO₂ low-pressure gas adsorption. At the immature stage, the samples with high OM content are characterized by lower porosity than the organic-matter-lean samples. At this stage, high OM content leads to the disruption of stiffer mineral framework; mixed organic-mineral framework is more prone to mechanical compaction than mineral framework. At the oil window stage, porosity of OM-rich samples declines due to pore-throat plugging and pore filling by bitumen. At the wet and dry gas generation stage, porosity of OM-rich samples increases mainly due to pore-throats unplugging. Absent or weak correlation between porosity and OM content at the wet and dry gas stages indicates poor development of OM-hosted secondary porosity. High contents of clay minerals in the studied samples fail to provide the rigid mineral framework and pressure shadows necessary for OM-hosted secondary porosity development.

1. Introduction

The reservoir quality of gas shales from unconventional reservoirs in low-permeability shales largely depends on pore systems for storing and releasing hydrocarbon gas. It has also been well accepted that the behavior of shales as a source/reservoir rock for gas is influenced not only by storage mechanisms operating via mineral components (e.g., displacement phenomena and hydrodynamic solubility, Bruant Jr. et al., 2002) but even more importantly, by characteristics of organic matter (OM) offering sorption sites on the surface area of mesopores or "volume filling" in micropores of OM (Bustin et al., 2008).

In general, mineral composition, OM content and type, thermal maturity, and textural and structural features of rocks all control the development of porosity networks in mudstones (i.e., Grathoff et al., 2016; Loucks et al., 2012; Milliken and Olson, 2017; Schieber et al., 2016; Valenza et al., 2013). The influence of OM thermal maturity on the pore systems has been widely discussed over the last few decades. In addition to the original rock characteristics, maturity-related secondary processes such as hydrocarbon generation, cracking, and formation of

solid bitumen exert unique influences on the porosity of shales (Jarvie et al., 2007; Loucks et al., 2009). For example, for the OM-rich Upper Devonian New Albany Shale (TOC range 1.2–13.0 wt%), Mastalerz et al. (2013) suggested that maturity exerted the dominant control on the development of porosity, masking the effects of compositional differences. Specifically, they observed: 1) total porosity reduction during the transition from mature to late-mature shale; (2) a large increase in total pore volumes between R_0 1.15 % and 1.41 %, witnessing generation of new pores, and (3) rearrangement in the proportions of pore sizes. Mastalerz et al. (2013) attributed those changes to structural modifications of OM in response to hydrocarbon generation and migration.

The influence of OM content on pore systems in shales has also been often mentioned, although with a caveat that it is difficult to separate the influence of OM abundances from other influencing factors. Generally, a positive correlation between OM content and total porosity, or between OM content and micropore or mesopore volumes, is expected (Chalmers and Bustin, 2007; Clarkson et al., 2013; Milliken et al., 2013; Ross and Bustin, 2009; Strapoć et al., 2010). However, these correlations may be obstructed by the strong influence of other factors e.g.,

E-mail address: grzegorz.lis@uwr.edu.pl (G.P. Lis).

^{*} Corresponding author.

mineralogical composition and thermal maturity (Mastalerz et al., 2013).

This study addresses the influence of OM on porosity in Silurian shales of the Baltic Basin in Poland. The Early Paleozoic successions in the Polish part of the Baltic Basin were regarded as important hydrocarbon source rocks and unconventional resource play. Therefore, several studies provided characterization of these rocks in terms of their mineralogical composition, OM content, thermal maturity, porosity, and permeability (Karnkowski, 2007; Milliken et al., 2018; Poprawa, 2010; Porębski et al., 2013; Siomski et al., 2021; Topór et al., 2017a, 2017b). Although the influence of OM content was mentioned or discussed in the majority of those studies, the present study benefits from the availability of a unique set of samples that allowed separation into low-, medium-, and high-OM content groups, and investigates the evolution of porosity with increasing maturation from immature to deeply overmature stages. As such, this study offers a new perspective on the Silurian shales as gas reservoirs.

2. Geological setting

The Baltic Basin is an Early Paleozoic sedimentary basin developed in the southwestern part of the East European Craton (Fig. 1). It is bounded by the Baltic Shield to the north, the Mazury-Belarus High to the south and southeast, the Teisseyre-Tornquist Zone (TTZ) to the southwest, and the Caledonian Deformation Front to the west (Mazur et al., 2015; Poprawa et al., 1999; Ziegler, 1990). The Baltic Basin was established as a passive margin during the Late Vendian and Cambrian and developed into a foreland basin by the Late Ordovician and Silurian (Nawrocki and Poprawa, 2006; Poprawa et al., 1999). A tectonic collision between Eastern Avalonia and Baltica tectonic plates affected sedimentation rates and burial diagenesis, which varied from east to west (Poprawa et al., 1999). The thickness of Lower Paleozoic sediments increases westward, reaching several thousand meters near the TTZ (Modliński et al., 1999).

The OM-rich shales and mudstones of this study were deposited

during the Upper Ordovician and Lower Silurian in an anoxic foreland basin environment, driven by a transgression of the early Llandovery sea (Podhalańska, 2009). Tectonic subsidence curves indicate an acceleration of the subsidence rate near the Caledonian Deformation Front during the Lower Silurian (Llandovery-Wenlock) (Poprawa et al., 1999). Although the initial stage of subsidence did not lead to a significant increase in sediment thickness, it is characterized by a condensed facies of black shales rich in graptolites, typically 20-40 m thick, with some layers reaching up to 70 m (Podhalańska, 2009). The succession of sediment facies is parallel to TTZ facies zonation from deep-water black shales in the west to more carbonate-rich sediments in the east (Poprawa et al., 1999). The OM in these shales is predominantly planktonicbacterial, type II kerogen, reflecting uniform origins due to the absence of terrigenous plant input in the Early Silurian (Derkowski and Marynowski, 2016; Skret and Fabianska, 2009). Thermal maturity of the OM increases westward, ranging from immature to overmature (Skret and Fabianska, 2009).

2.1. Samples

Sample selection for the study aimed to cover a wide range of thermal maturity and OM content. Ninety-four samples were selected from the core material collected for previous studies (Topór et al., 2017a, 2017b; Topór et al., 2016). These samples represent lower Llandovery (Silurian) strata of shales and mudstones that cover a present-day depth range from ~1400 to ~4500 m. In addition, two samples were collected from a Silurian outcrop in the Holy Cross Mountains (Modliński and Szymański, 2001) at the western edge of the East European Craton.

3. Methods

3.1. Organic petrography

Samples for organic petrography were crushed to ≤ 2 mm rock chips, cold-mounted within epoxy resin to prepare petrographic pellets,

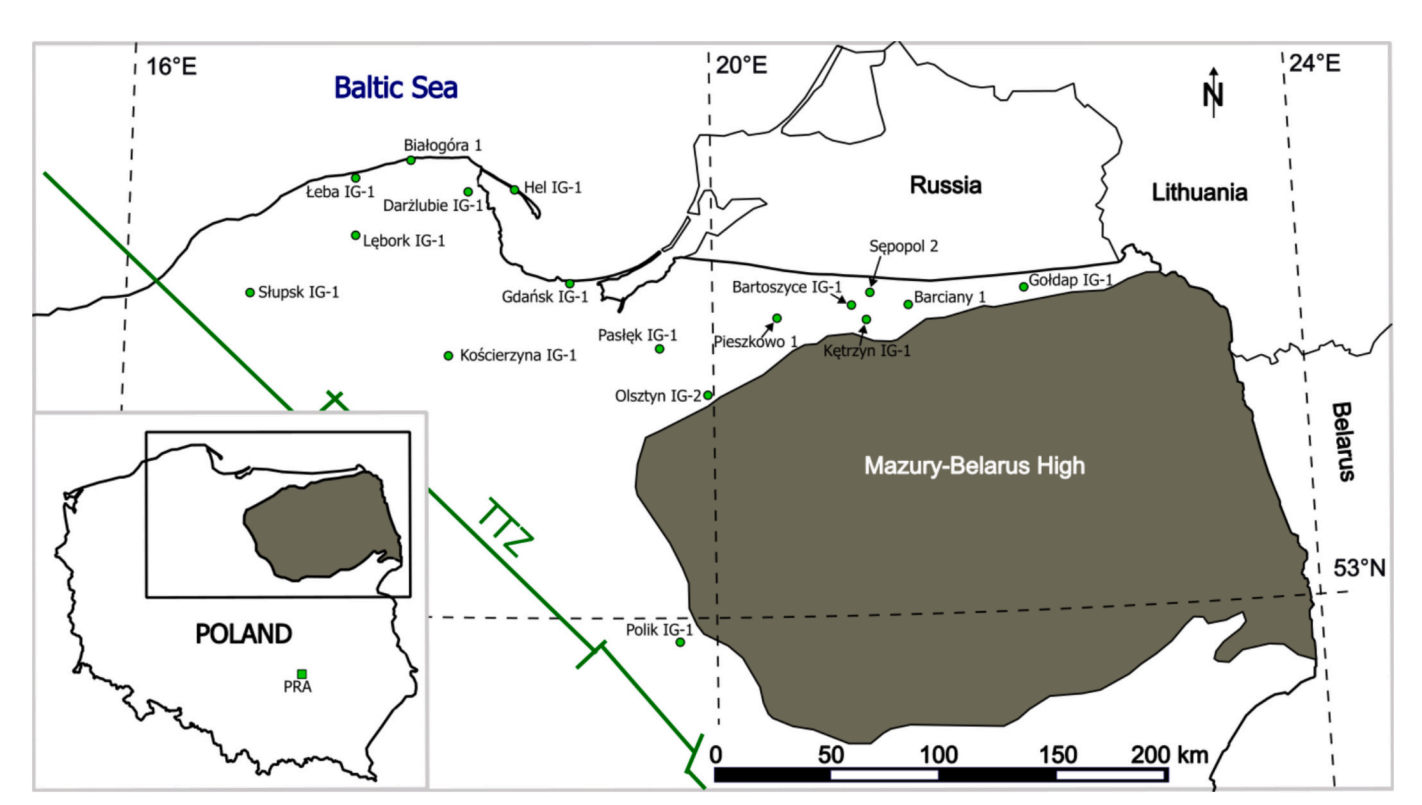


Fig. 1. Geological background of the study area (after Topór et al., 2017a) with the location of well (dots) and outcrop (square) samples. TTZ - Teisseyre-Tornquist Zone.

subsequently ground, and polished according to the ASTM D2797 (ASTM, 2015). An Axio Imager Z2 (ZEISS) reflected-light microscope coupled with a TIDAS S MSP 200 photometer (JM Microsystems GmbH) was used for reflectance measurements. The authors attempted to collect both graptolite and solid bitumen reflectance data. In order to maximize the number of samples with reflectance measurements, a $100 \times$ lens was used rather than a more common 50× objective. Using the larger magnification allowed for the measurement of small solid bitumen particles and very thin graptolites that were too small to be measured with a $50\times$ lens. In several samples with very low OM content, it was impossible to obtain reflectance data. Thermal maturity for these samples is estimated based on the extrapolation of reflectance data from other samples from the same well. Vitrinite reflectance equivalent (VRE) was calculated from graptolite reflectance according to Petersen et al. (2013). The only exception is sample SE2, a single sample from its parent well; it does not contain graptolites. The VRE for this sample was estimated based on solid bitumen reflectance using the Schoenherr et al. (2007) equation.

3.2. OM content

OM content is expressed using total organic carbon (TOC). The TOC was measured using Rock-Eval 6 Vinci Technologies.

3.3. Gas sorption

Low-pressure gas sorption experiments with CO2 and N2 were conducted on an Anton-Paar NOVAtouchLX4 surface area and pore size analyzer. Samples were ground to pass through the 0.25 mm sieve and subsequently degassed for 12 h at 110 °C in a vacuum to remove moisture and a majority of hydrocarbons from the pore network. The degassing temperature was chosen to remove the free water, light- and medium-weight hydrocarbons and, at the same time, to minimize clay interlayer dehydration, leading to the shrinking of clay particles and thermal changes within OM, especially in the immature and lowmaturity samples. CO₂ isotherms were collected at 0.0 °C (273.1 °C) in the 2.75-750 mmHg pressure range, corresponding to 0.30-1.47 nm pore diameter with 36 adsorption points. N₂ isotherms were collected at liquid nitrogen temperature (77.3 K) in the 36-755 mmHg pressure range, corresponding to the 1.35-160 nm pore diameter with 39 adsorption and 19 desorption points. Quantachrome TouchWin software was used to determine surface areas, total pore volumes, pore size distributions, and to generate adsorption and desorption isotherms according to the Brunauer-Emmett-Teller (BET), Barrett-Joyner-Halenda (BJH), Dubinin-Radushkevich (DR), and density functional theory (DFT) methods. Definitions and discussion of these parameters are given elsewhere (Gregg and Sing, 1982). In this paper, the classification of the pores into micropores (less than 2 nm), mesopores (2-50 nm), and macropores (greater than 50 nm) follows that of the International Union of Pure and Applied Chemistry (Orr, 1977; Rouquerol et al., 1994).

4. Results

4.1. Organic petrography

Out of 96 studied samples, 69 samples contain graptolites, and 48 contain solid bitumen particles suitable for reflectance measurements. Overall thermal maturity varies from 0.40 to 4.62 % VRE (Table 1), with three immature samples (<0.5 % VRE), 26 samples of low maturity (\ge 0.5 to <0.75 % VRE), 34 samples within the oil window (\ge 0.75 to <1.1 % VRE), 12 samples within the wet gas window (\ge 1.1 to <1.4 % VRE), 11 samples within the dry gas window (\ge 1.4 to <2.0 % VRE), and 10 overmature samples (\ge 2.0 % VRE). Maceral composition (Fig. 2) of the immature and early oil window samples is dominated by bituminite, often constituting more than 50 vol% observable OM; alginite is the second most common maceral, averaging about 20 vol% of organic

particles; liptodetrinite is present in smaller amounts (a few to several vol%). The percentage of liptinite group macerals gradually decreases between 0.7 and 1.05 % VRE, with bituminite disappearing at 0.91 % VRE, slightly earlier than alginite and liptodetrinite (at 1.05 % VRE). Solid bitumen is rare in immature and early oil window samples (few to several vol%) and gradually increases in volume through the oil window as a result of conversion of macerals from the liptinite group (Hackley et al., 2018; Jacob, 1989; Liu et al., 2019) to dominate OM maceral composition from the peak oil window through higher maturities. Graptolites, when present, range from a few to 30 vol% of the total OM with no obvious volumetric trends with increasing maturity. Chitinozoans and acritarchs were observed in small amounts in several samples.

4.2. OM content

The TOC content of the samples ranges from 0.10 to 10.29 wt%, with the TOC values gradually decreasing with maturity. The decrease is steeper in the immature stage through the oil and wet gas windows and gentler in the dry gas window and overmature samples. In order to better visualize and explain the TOC influence on porosity changes with maturity, samples were clustered into three groups based on OM content. The partition into high-, medium- and low-TOC sample groups, roughly 2.0 and 4.5 wt% TOC at 0.5 % VRE, takes into account decreasing TOC value with maturity, as presented in Fig. 3.

4.3. Gas sorption data

4.3.1. Total pore volume

The total pore volume (TPV) values were calculated by adding the micropore volume obtained from CO₂ adsorption (encompassing pore size from 0.30 to 1.47 nm in diameter), mesopores, and macropore volume determined by N2 adsorption (1.47 to 169 nm in diameter). The TPV (Fig. 4, Table 1) for the immature and low-maturity samples shows a wide spread in values between 0.04 and 0.10 cc/g, with the high-TOC group having the lowest values among the three groups. With increasing maturity, the TPV of all the samples decreases to roughly 1 % VRE, where the medium- and high-TOC groups reached the TPV between 0.015 and 0.03 cc/g, separating from the low-TOC samples. A further increase in maturity through the wet gas window registers an increase in TPV for the medium- and high-TOC groups, with a local maximum in TPV at 0.03–0.04 cc/g between 1.5 and 2.0 % VRE, where the mediumand high-TOC samples merge with the low-TOC group. A subsequent increase in maturity results in a slight decrease for all the groups, with the TPV values in the range between 0.02 and 0.03 cc/g above 4.0 %

4.3.2. Micropore, mesopore, and macropore volumes

Micropore volume was calculated by adding pore volumes from CO_2 adsorption (encompassing pore size diameter between 0.30 and 1.47 nm) and pore volumes from N_2 adsorption between 1.47 and 2.0 nm. Mesopore and macropore volumes were calculated based on N_2 adsorption data in the range of 2.0–50.0 nm and 50–169 nm, respectively.

Micropore volume (Fig. 5A, B and Table 1) ranges between 0.0013 and 0.011 cc/g. It decreases from the immature and early mature stages to the oil window, increases through the wet gas window, and then decreases with a further increase in maturity. Overall, the trend is similar to TPV, but with more scatter. Although micropore volumes are initially decreasing with maturity like TPV and other pores, their decrease is slowest, as the percentage of micropores in TPV is increasing (Fig. 5B). The percentage of micropore volume within the TVP is highest on the high-TOC samples, indicating affinity between micropores and OM. Micropores have the lowest contribution to pore volume, ranging between 6 and 31 % of TPV.

Mesopore volume (Fig. 5C,D and Table 1) ranges between 0.0091 and 0.059 cc/g, and it is the dominant pore type, accounting for 45–73

Table 1

TOC, reflectance and adsorption parameters for the studied samples (vitrinite reflectance equivalent VRE, solid bitumen reflectance SB Ro, graptolite reflectance GR Ro, pore volume PV, total pore volume TPV, surface area SA). * indicates VRE was estimated based on VRE values for the neighboring samples from the same well; ** indicates VRE was calculated based on SB Ro; for all the other samples, VRE values were calculated based on GR Ro.

| Sample name | Well name | TOC | VRE | SB Ro | GR Ro | PV <2 nm | PV 2-50 nm | PV >50 nm | TPV | BET SA | CO ₂ SA |
|-----------------|-----------------|--------------|--------|-------|-------|--------------------|------------|------------------|------------------|--------------|--------------------|
| | | (wt%) | (%) | (%) | (%) | (cc/g) | (cc/g) | (cc/g) | (cc/g) | (m^2/g) | (m^2/g) |
| GO8 | | 1.78 | 0.40 | _ | 0.32 | 0.00532 | 0.0425 | 0.0109 | 0.0587 | 20.27 | 0.0045 |
| GO7 | | 1.49 | 0.55 | 0.31 | 0.53 | 0.00657 | 0.0580 | 0.0204 | 0.0849 | 27.78 | 0.0041 |
| GO5 | | 2.88 | 0.48 | _ | 0.43 | 0.00650 | 0.0424 | 0.0112 | 0.0600 | 22.58 | 0.0043 |
| GO4 | | 2.42 | 0.54 | 0.27 | 0.52 | 0.00611 | 0.0469 | 0.0118 | 0.0648 | 24.16 | 0.0041 |
| GO2 | | 0.21 | *0.52 | _ | _ | 0.00723 | 0.0494 | 0.0132 | 0.0698 | 28.88 | 0.0055 |
| GO1 | | 6.39 | 0.50 | - | 0.47 | 0.00942 | 0.0308 | 0.0081 | 0.0482 | 14.38 | 0.0051 |
| Goldap IG-1 | Gołdap IG-1 | 4.83 | 0.48 | - | 0.43 | 0.00581 | 0.0366 | 0.0113 | 0.0536 | 16.59 | 0.0039 |
| KE7 | | 1.41 | *0.58 | 0.55 | - | 0.00744 | 0.0503 | 0.0116 | 0.0694 | 27.65 | 0.0050 |
| KE6 | | 3.97 | 0.57 | _ | 0.56 | 0.00917 | 0.0532 | 0.0253 | 0.0876 | 29.51 | 0.0058 |
| KE5 | | 3.44 | 0.62 | 0.44 | 0.63 | 0.00798 | 0.0423 | 0.0221 | 0.0723 | 20.84 | 0.0046 |
| KE4 | | 4.95 | 0.55 | 0.21 | 0.55 | 0.00633 | 0.0309 | 0.0114 | 0.0486 | 14.46 | 0.0043 |
| KE3 | | 1.55 | 0.56 | 0.33 | 0.55 | 0.00680 | 0.0384 | 0.0162 | 0.0614 | 20.33 | 0.003 |
| Kętrzyn IG-1 | Kętrzyn IG-1 | 7.14 | 0.60 | 0.31 | 0.60 | 0.00837 | 0.0353 | 0.0115 | 0.0551 | 18.82 | 0.004 |
| BA4 | | 0.99 | 0.59 | 0.48 | 0.59 | 0.00805 | 0.0548 | 0.0201 | 0.0830 | 26.38 | 0.0059 |
| BA2 | Barciany 1 | 2.92 | 0.66 | 0.42 | 0.69 | 0.00853 | 0.0589 | 0.0258 | 0.0932 | 27.81 | 0.0053 |
| BT9 | | 1.68 | 0.54 | 0.48 | 0.53 | 0.00685 | 0.0493 | 0.0116 | 0.0677 | 26.04 | 0.0050 |
| BT8 | | 1.26 | 0.64 | _ | 0.66 | 0.00625 | 0.0446 | 0.0123 | 0.0632 | 23.67 | 0.0053 |
| BT7 | | 0.42 | 0.66 | - | 0.68 | 0.00601 | 0.0424 | 0.0142 | 0.0626 | 23.77 | 0.0041 |
| BT6 | | 1.31 | *0.65 | 0.97 | - | 0.00661 | 0.0514 | 0.0126 | 0.0706 | 27.04 | 0.0047 |
| BT5 | | 3.57 | 0.65 | - | 0.68 | 0.00422 | 0.0453 | 0.0132 | 0.0628 | 26.00 | 0.004 |
| Bartoszyce IG-1 | Bartoszyce IG-1 | 10.29 | 0.56 | - | 0.55 | 0.01096 | 0.0349 | 0.0123 | 0.0582 | 17.37 | 0.0080 |
| SE2 | Sępopol 2 | 0.66 | **0.69 | 0.48 | - | 0.00703 | 0.0576 | 0.0171 | 0.0817 | 29.59 | 0.0048 |
| PI9 | | 1.11 | *0.7 | 0.94 | _ | 0.00658 | 0.0407 | 0.0158 | 0.0631 | 22.68 | 0.0040 |
| PI8s | | 2.83 | 0.72 | _ | 0.77 | 0.00527 | 0.0368 | 0.0148 | 0.0568 | 17.05 | 0.0031 |
| PI7 | | 0.24 | *0.70 | _ | _ | 0.00692 | 0.0474 | 0.0113 | 0.0657 | 27.35 | 0.0046 |
| PI4 | | 0.13 | *0.70 | - | - | 0.00755 | 0.0501 | 0.0193 | 0.0770 | 30.38 | 0.0049 |
| PI3 | | 2.80 | 0.69 | _ | 0.72 | 0.00789 | 0.0469 | 0.0127 | 0.0675 | 27.25 | 0.0043 |
| PI2 | | 6.46 | 0.70 | - | 0.74 | 0.00745 | 0.0299 | 0.0107 | 0.0481 | 16.41 | 0.0047 |
| PI1 | Pieszkowo 1 | 8.54 | 0.70 | - | 0.74 | 0.00853 | 0.0340 | 0.0080 | 0.0504 | 18.41 | 0.0061 |
| OL5 | | 0.66 | 0.91 | 0.97 | 1.03 | 0.00558 | 0.0269 | 0.0103 | 0.0427 | 15.30 | 0.0041 |
| OL1 | Olsztyn IG-2 | 0.12 | *0.91 | - | - | 0.00693 | 0.0338 | 0.0092 | 0.0500 | 23.46 | 0.0052 |
| PA5 | | 0.24 | *0.88 | - | - | 0.00565 | 0.0269 | 0.0084 | 0.0410 | 19.32 | 0.0039 |
| PA4 | | 2.25 | 0.97 | - | 1.11 | 0.00573 | 0.0212 | 0.0082 | 0.0351 | 12.21 | 0.0042 |
| PA3 | | 1.33 | 0.79 | - | 0.86 | 0.00408 | 0.0236 | 0.0110 | 0.0387 | 11.55 | 0.0027 |
| PA1 | Pasłęk IG-1 | 0.57 | *0.88 | - | - | 0.00542 | 0.0275 | 0.0102 | 0.0431 | 18.65 | 0.0039 |
| PRA1 | | 1.33 | 0.85 | 0.86 | 0.95 | 0.00255 | 0.0132 | 0.0069 | 0.0226 | 5.60 | 0.0023 |
| PRA2 | Outcrop samples | 1.37 | *0.85 | 0.87 | - | 0.00357 | 0.0129 | 0.0058 | 0.0224 | 6.50 | 0.0029 |
| HE10 | | 0.19 | *0.90 | - | - | 0.00518 | 0.0190 | 0.0047 | 0.0289 | 16.08 | 0.0044 |
| HE9 | | 0.64 | *0.90 | _ | _ | 0.00400 | 0.0254 | 0.0089 | 0.0383 | 18.51 | 0.0040 |
| HE7 | | 6.30 | 0.84 | _ | 0.93 | 0.00531 | 0.0105 | 0.0057 | 0.0215 | 3.84 | 0.0040 |
| HE6 | | 8.14 | 1.00 | 0.51 | 1.24 | 0.00602 | 0.0119 | 0.0048 | 0.0227 | 4.32 | 0.0044 |
| HE5 | | 0.62 | *0.90 | 1.36 | - | 0.00540 | 0.0238 | 0.0051 | 0.0343 | 14.61 | 0.0042 |
| HE4 | | 2.81 | 0.94 | - | 1.07 | 0.00382 | 0.0179 | 0.0081 | 0.0297 | 7.74 | 0.0032 |
| HE3 | | 2.84 | 0.97 | - | 1.11 | 0.00443 | 0.0180 | 0.0106 | 0.0330 | 6.51 | 0.0022 |
| HE2 | | 0.48 | *0.90 | - | - | 0.00368 | 0.0168 | 0.0054 | 0.0259 | 11.98 | 0.0023 |
| HE1 | Hel IG-1 | 7.22 | 0.86 | 0.48 | 0.96 | 0.00659 | 0.0100 | 0.0055 | 0.0221 | 4.11 | 0.0042 |
| DA13 | | 0.75 | 1.07 | 1.36 | 1.24 | 0.00482 | 0.0209 | 0.0079 | 0.0336 | 14.39 | 0.0035 |
| DA12 | | 0.81 | *1.00 | - | - | 0.00408 | 0.0190 | 0.0085 | 0.0316 | 11.43 | 0.0035 |
| DA10 | | 0.18 | *1.00 | 1.13 | - | 0.00474 | 0.0184 | 0.0081 | 0.0312 | 14.83 | 0.0032 |
| DA8 | | 0.19 | *1.00 | - | - | 0.00539 | 0.0224 | 0.0100 | 0.0378 | 16.94 | 0.0037 |
| DA7 | | 0.22 | *1.00 | - | - | 0.00621 | 0.0216 | 0.0054 | 0.0331 | 19.37 | 0.0047 |
| DA6 | | 0.47 | 1.01 | 0.82 | - | 0.00648 | 0.0267 | 0.0140 | 0.0472 | 19.75 | 0.004 |
| DA5 | | 6.72 | 0.94 | - | 1.16 | 0.00607 | 0.0091 | 0.0042 | 0.0194 | 3.45 | 0.004 |
| DA4 | | 4.69 | 1.04 | - | 1.20 | 0.00574 | 0.0209 | 0.0086 | 0.0352 | 12.67 | 0.003 |
| DA3 | | 1.42 | 1.17 | 1.44 | 1.38 | 0.00340 | 0.0193 | 0.0111 | 0.0339 | 7.25 | 0.001 |
| DA2 | | 2.79 | 0.97 | - | 1.11 | 0.00410 | 0.0164 | 0.0105 | 0.0310 | 5.98 | 0.002 |
| DA1 | | 4.15 | 1.05 | - | 1.22 | 0.00450 | 0.0144 | 0.0052 | 0.0240 | 6.32 | 0.002 |
| DA0r | | 4.30 | 1.01 | 1.25 | 1.17 | 0.00595 | 0.0142 | 0.0070 | 0.0272 | 5.23 | 0.003 |
| DA0 | Darżlubie IC 1 | 5.22 6.41 | 1.01 | _ | 1.16 | 0.00563 0.00515 | 0.0141 | 0.0064 0.0041 | 0.0261 0.0197 | 6.17 4.21 | 0.004 |
| Dar-1 | Darżlubie IG-1 | 6.41 | 1.04 | | 1.19 | | 0.0104 | | | 4.21 | 0.0032 |
| BG8 | | 0.44 | 1.11 | 1.37 | 1.30 | 0.00552 | 0.0198 | 0.0105 | 0.0358 | 16.01 | 0.0043 |
| BG7 | | 0.24 | *1.05 | | - | 0.00536 | 0.0204 | 0.0117 | 0.0374 | 14.76 | 0.0036 |
| BG6 | Białogóra 1 | 7.45 | 1.03 | - | 1.19 | 0.00687 | 0.0120 | 0.0041 | 0.0230 | 4.98 | 0.0046 |
| BG5 | | 5.38 | 1.05 | 1.02 | 1.22 | 0.00469 | 0.0117 | 0.0059 | 0.0223 | 4.25 | 0.0034 |

(continued on next page)

Table 1 (continued)

| Sample name | Well name | TOC (wt%) | (%) | SB Ro (%) | GR Ro | $\frac{PV < 2 \text{ nm}}{(cc/g)}$ | PV 2–50 nm (cc/g) | $\frac{PV > 50 \text{ nm}}{(cc/g)}$ | TPV (cc/g) | $\frac{\text{BET SA}}{(\text{m}^2/\text{g})}$ | $\frac{\text{CO}_2 \text{ SA}}{(\text{m}^2/\text{g})}$ |
|-------------|------------------|-----------|-------|--------------|-------|------------------------------------|-------------------|-------------------------------------|------------|---|--|
| | | | | | (%) | | | | | | |
| BG1 | | 2.49 | 1.11 | 1.17 | 1.30 | 0.00450 | 0.0141 | 0.0052 | 0.0237 | 5.86 | 0.0033 |
| LB8 | | 0.59 | 1.21 | - | 1.43 | 0.00361 | 0.0176 | 0.0077 | 0.0289 | 10.96 | 0.0022 |
| LB5 | | 0.36 | *1.20 | _ | _ | 0.00452 | 0.0211 | 0.0088 | 0.0344 | 13.43 | 0.0032 |
| LB4 | | 5.51 | 1.31 | 0.68 | 1.57 | 0.00497 | 0.0136 | 0.0051 | 0.0237 | 5.99 | 0.0032 |
| LB3 | | 3.53 | 1.18 | 1.15 | 1.40 | 0.00195 | 0.0145 | 0.0069 | 0.0234 | 5.15 | 0.0006 |
| LB1 | Łeba IG-1 | 2.74 | 1.10 | 1.05 | 1.28 | 0.00127 | 0.0119 | 0.0052 | 0.0184 | 4.22 | 0.0003 |
| GD7 | | 1.81 | 1.23 | - | 1.47 | 0.00368 | 0.0220 | 0.0081 | 0.0339 | 9.75 | 0.0019 |
| GD3 | | 0.10 | *1.20 | _ | _ | 0.00551 | 0.0214 | 0.0070 | 0.0339 | 17.14 | 0.0042 |
| GD2 | | 1.03 | 1.12 | 1.51 | 1.32 | 0.00664 | 0.0239 | 0.0130 | 0.0435 | 16.55 | 0.0046 |
| GD1 | | 0.38 | *1.20 | - | - | 0.00577 | 0.0248 | 0.0102 | 0.0408 | 17.27 | 0.0041 |
| GD8 | Gdańsk IG-1 | 2.21 | 1.27 | - | 1.52 | 0.00504 | 0.0154 | 0.0092 | 0.0296 | 5.38 | 0.0036 |
| LE9 | | 0.93 | 1.94 | 2.44 | 2.43 | 0.00590 | 0.0190 | 0.0077 | 0.0325 | 15.55 | 0.0059 |
| LE8 | | 0.65 | 1.70 | 2.32 | 2.11 | 0.00497 | 0.0173 | 0.0043 | 0.0265 | 13.89 | 0.0037 |
| LE7 | | 0.23 | *1.82 | - | _ | 0.00491 | 0.0210 | 0.0076 | 0.0335 | 14.82 | 0.0031 |
| LE3 | | 1.72 | 1.85 | 2.52 | 2.32 | 0.00520 | 0.0192 | 0.0084 | 0.0328 | 12.79 | 0.0037 |
| LE-11 | Lębork IG-1 | 1.93 | 1.66 | 2.05 | 2.06 | 0.00525 | 0.0210 | 0.0080 | 0.0342 | 13.27 | 0.0037 |
| KO14 | | 1.80 | 1.94 | 1.45 | 2.44 | 0.00521 | 0.0194 | 0.0066 | 0.0312 | 14.94 | 0.0033 |
| KO9 | | 0.34 | *1.90 | - | - | 0.00518 | 0.0200 | 0.0087 | 0.0338 | 15.84 | 0.0035 |
| KO6 | | 0.38 | 1.78 | 2.29 | 2.23 | 0.00689 | 0.0239 | 0.0092 | 0.0399 | 18.69 | 0.0052 |
| KO5 | | 1.91 | 1.66 | 2.29 | 2.23 | 0.00585 | 0.0221 | 0.0093 | 0.0373 | 15.76 | 0.0034 |
| KO4 | | 4.97 | 2.00 | 1.76 | 2.52 | 0.00923 | 0.0236 | 0.0061 | 0.0389 | 17.45 | 0.0061 |
| KO2 | Kościerzyna IG-1 | 1.57 | 1.82 | 2.34 | 2.27 | 0.00604 | 0.0190 | 0.0085 | 0.0335 | 16.21 | 0.0046 |
| SL7 | | 0.71 | 2.61 | 4.20 | 3.35 | 0.00400 | 0.0148 | 0.0069 | 0.0257 | 9.82 | 0.0027 |
| SL5 | | 1.49 | 3.32 | 3.74 | 5.78 | 0.00353 | 0.0116 | 0.0052 | 0.0204 | 8.26 | 0.0029 |
| SL3 | | 1.53 | *2.65 | 3.63 | - | 0.00241 | 0.0121 | 0.0069 | 0.0215 | 6.17 | 0.0015 |
| SL10 | Słupsk IG-1 | 0.87 | 2.66 | 3.88 | 3.42 | 0.00392 | 0.0150 | 0.0084 | 0.0273 | 9.69 | 0.0031 |
| PO8 | | 1.31 | 4.14 | 4.55 | 5.45 | 0.00233 | 0.0169 | 0.0090 | 0.0282 | 8.65 | 0.0026 |
| PO7 | | 1.71 | 4.17 | 4.45 | 5.49 | 0.00279 | 0.0124 | 0.0047 | 0.0198 | 6.13 | 0.0012 |
| PO6 | | 1.74 | 4.62 | 4.80 | 6.10 | 0.00343 | 0.0140 | 0.0048 | 0.0222 | 9.38 | 0.0021 |
| PO4 | | 0.45 | *4.30 | - | - | 0.00327 | 0.0155 | 0.0072 | 0.0259 | 9.23 | 0.0024 |
| PO2 | Polik IG-1 | 3.46 | 4.19 | 2.92 | 5.52 | 0.00587 | 0.0179 | 0.0063 | 0.0300 | 11.53 | 0.0043 |
| PO1 | rollk IG-1 | 2.71 | 4.46 | _ | 5.89 | 0.00558 | 0.0154 | 0.0060 | 0.0270 | 10.04 | 0.0036 |

% TPV. Macropore volume (Fig. 5E, F and Table 1) ranges between 0.0041 and 0.026 cc/g, constituting 14 to 34 % of TPV. Both mesopore and macropore volumes follow trends similar to TPV for all three sample types.

4.3.3. Surface area

The BET surface area from N2 isotherms of the immature and low maturity samples ranges between 14 and 30 m²/g, with high-TOC samples having the lowest values and mid- to low-TOC samples grouped together with higher values (Fig. 6). With increasing maturity, BET surface areas are following different evolution paths for different sample types. For low-TOC samples, surface areas decrease to the 10 to 20 m²/g range at the oil window and down to $\sim 10 \text{ m}^2/\text{g}$ for the overmature samples. Medium-TOC samples experience the biggest decline in surface area from immature to the end of the oil window, dropping from 20 to 30 m²/g to 4-10 m²/g for the majority of the samples, whereas high-TOC samples drop from 14 to 20 to 3-6 m²/g and have the lowest BET surface area values among the three sample types. A subsequent maturity increase results in a rebound in BET surface area values for the mid and high-TOC samples to 13–17 m²/g around 2.0 % VRE. Further maturity increase (2.0 to 4.5 % VRE) results in a slow decrease in surface areas for all sample types.

Surface area calculated using the DFT method for the $\rm CO_2$ adsorption isotherms ($\rm CO_2$ SA) ranges between 1 and 25 m²/g (Fig. 7). Immature and low-maturity samples are characterized by $\rm CO_2$ SA in the $\rm 11-25$ m²/g range. Although all data for the three sample groups overlap, the three points with the highest $\rm CO_2$ SA belong to the high-TOC group. A maturity increase to and slightly past the oil window (1.2 % VRE) leads to a decline in the $\rm CO_2$ SA for all three groups, with the greatest decline (down to the minimum at $\rm 1-2$ m²/g) for the mid-TOC samples. A further maturity increase leads to a steep increase within the 1.2 to 2.0 % VRE

range, followed by a shallower decline past 2.0 % VRE in CO_2 SA. The high-TOC group exhibits higher CO_2 SA values for the overmature samples than the mid- and low-TOC groups.

5. Discussion

The studied formation was a target for shale gas production in the past, but after several years of exploration, it was considered to be a poor reservoir, and exploration efforts were aborted (Hendel et al., 2015). The following discussion will attempt to identify the main factors affecting porosity evolution within the studied reservoir and the effects that porosity has on the reservoir quality. Specifically, the focus is on the impact of OM content on porosity evolution and discuss them in the context of processes occurring at various thermal maturity stages.

5.1. Immature and low-maturity (<0.75 % VRE) stages

It is well documented that compaction (both mechanical and chemical) is responsible for the overall decline in porosity with depth. Mondol et al. (2007) reviewed and presented porosity changes with depth for shales and argillaceous sediments from previous works. Their data show a decline in porosity from 40 to 80 % in fresh sediments to 10–40 % at 1 km, 5–30 % at 2 km, and less than 20 % at 4 km burial. Initially, mechanical compaction is the main driving force, but starting from a depth of approximately 2 km and temperatures above 70–80 °C, chemical compaction becomes dominant (Bjørlykke and Høeg, 1997; Mondol et al., 2008; Peltonen et al., 2009). In our study, this porosity trend is represented best by the low-TOC sample group (Fig. 4). TPV from a maximum of 0.09 cc/g at immature samples is steeply declining to 0.03–0.05 cc/g around the oil window.

Samples with increased OM content behave differently; this is

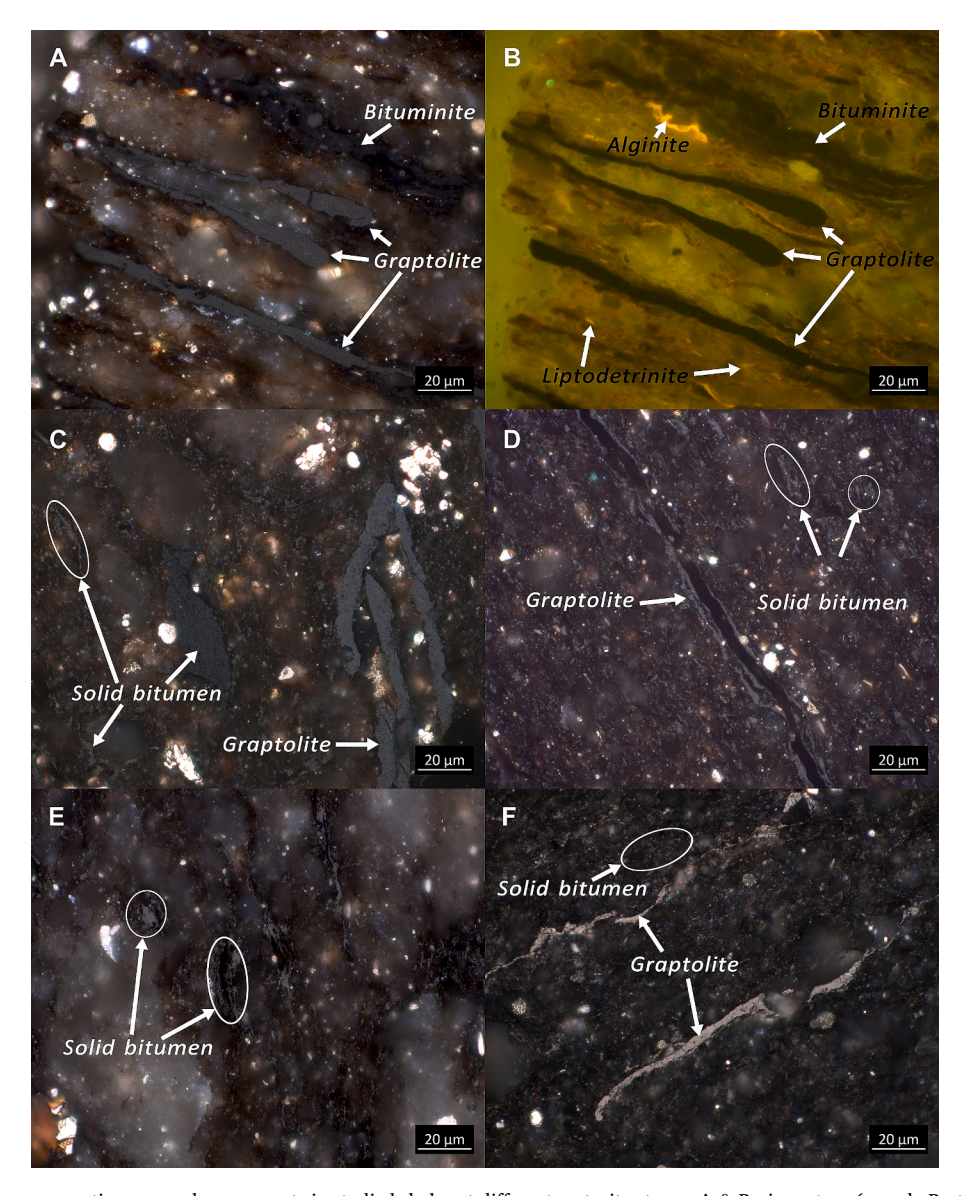


Fig. 2. Photomicrographs representing maceral components in studied shales at different maturity stages: A & B - immature (sample Bartoszyce IG-1, 0.56 % VRE, reflected and UV light, respectively), C - oil window (sample DA0, 1.01 % VRE), D - wet gas (sample LB4, 1.31 % VRE), E - dry gas (sample LE8, 1.70 % VRE), and F - overmature (sample PO2, 4.19 % VRE). All in oil immersion.

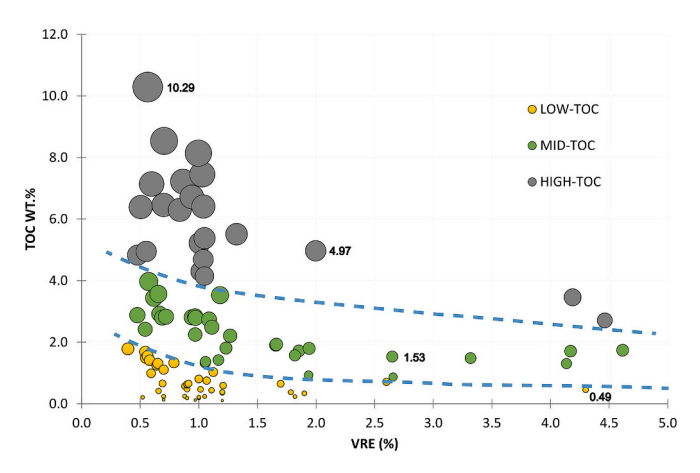


Fig. 3. Graph showing division of the studied samples into high-, mid-, and low-TOC sample groups across thermal maturity. Circle size represents TOC values with selected TOC provided in the figure.

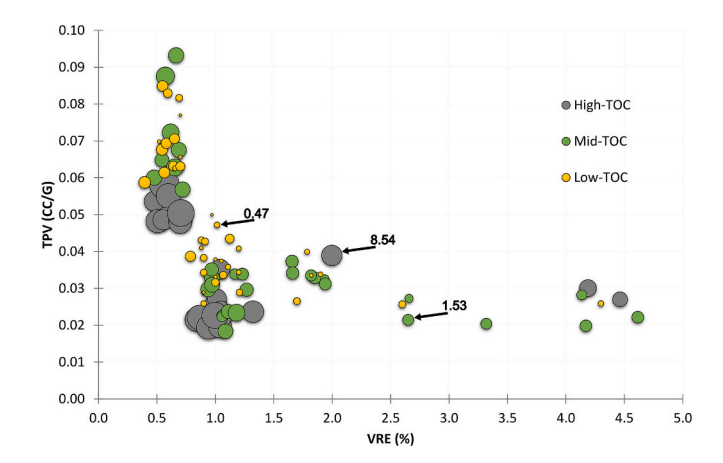


Fig. 4. TPV across thermal maturity for the three sample groups. Circle size represents TOC values with selected TOC provided in the figure.

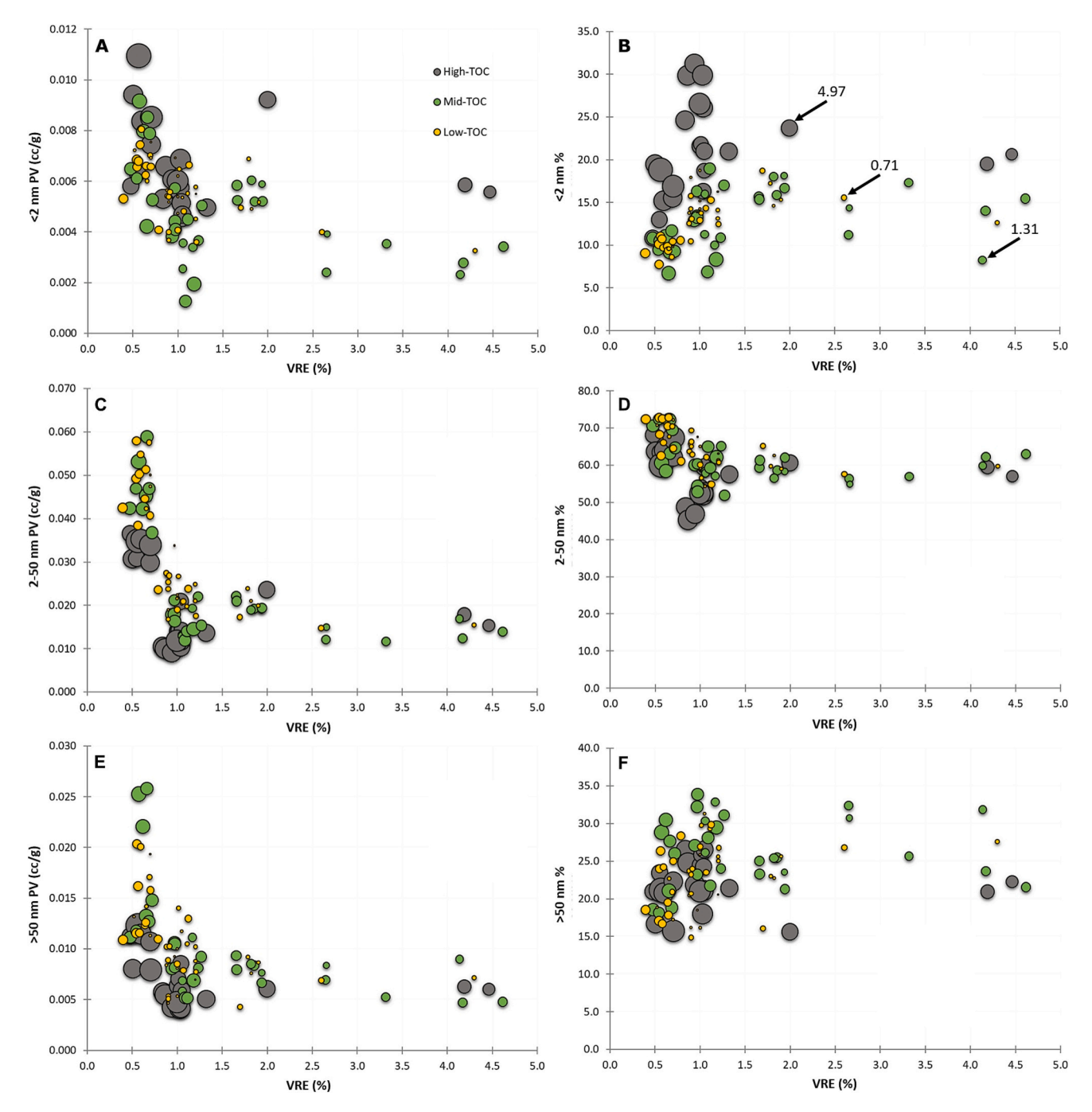


Fig. 5. Micro- (A, B), meso- (C, D) and macro- (E,F) pore volumes and percentages. Circle size represents TOC values with selected TOC provided on part B of the figure.

especially pronounced for the high-TOC sample group, which at this low maturity level is characterized by TPV values in the range of 0.048–0.058 cc/g—significantly lower than values for the low-TOC sample group (Figs. 4 and 8A). Microscopic observations show that solid bitumen at this early maturity stage is either not present or is present in small quantities (<10 vol% of total OM) in the form of pre-oil bitumen, forming distinct particles rather than pore-filling material. The small amount of hydrocarbon/bitumen generated at this maturity is likely absorbed within the kerogen network until a sorption potential is exceeded (Han et al., 2017; Jarvie, 2012a; Sandvik et al., 1992). Thus, the solid bitumen is unlikely to be responsible for the lower TPV in the high-TOC group at this maturity stage is related to the weak mechanical

properties of OM. OM is generally mechanically weaker than mineral constituents (Li et al., 2019), especially at low maturity, where OM is mechanically weakest, with mechanical stiffness increasing with maturity (Li et al., 2018a; Wang et al., 2022).

The fact that the low- and mid-TOC sample groups' TPV values overlap and only the high-TOC group plots separately (Fig. 4) suggests there is a certain threshold, in our case around 4.0–4.8 wt% TOC, above which resistance to mechanical compaction significantly decreases. The threshold value of 4.0–4.8 wt% TOC corresponds to roughly 10 % OM by volume and likely relates to the transition from the mainly rigid mineral matter framework, which effectively resists mechanical compaction, to the softer mixed mineral-organic framework with weak organic sites (Fig. 8A). Microscopic observations reveal that OM is not uniformly

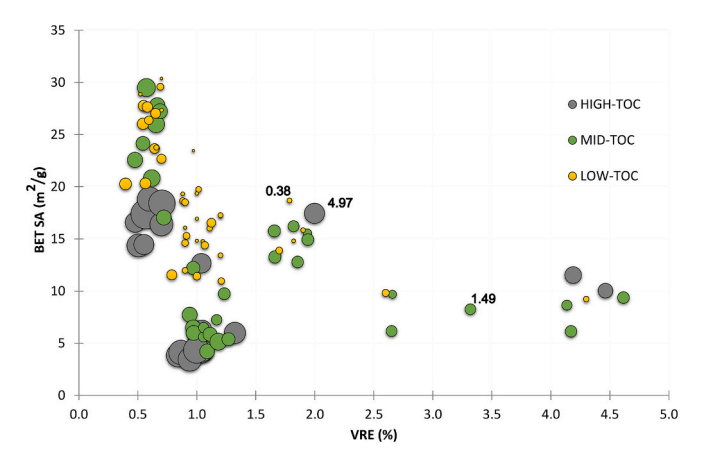


Fig. 6. BET surface area of three sample groups across maturity. Circle size represents TOC values with selected TOC provided in the figure.

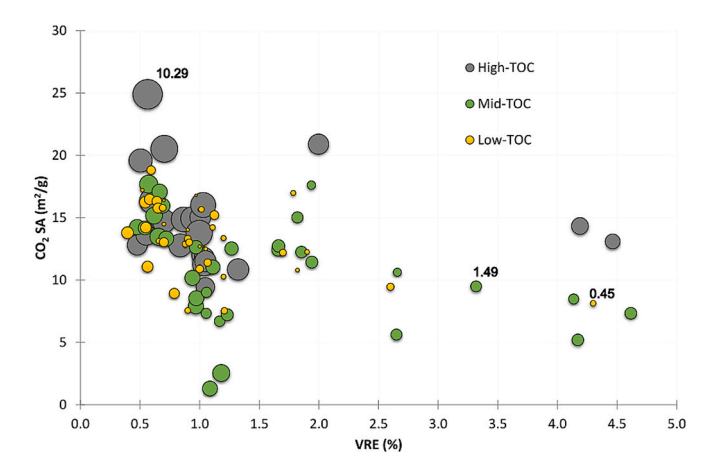


Fig. 7. $\rm CO_2$ surface area for the studied samples across maturity. Circle size represents TOC values with selected TOC provided in the figure.

dispersed through the rock matrix, but tends to concentrate in organic-rich layers several to tens of micrometers in thickness (Fig. 9). Increased concentration of OM in these layers further disrupts mineral framework, creating compaction-prone layers. The high-TOC group at maturity below 0.75 % VRE is characterized by a higher percentage of micropores, a similar percentage of mesopores, and a lower percentage of macropores compared to the other two sample groups (Fig. 5), meaning it has reduced pore size compared to two other groups. This is the result either of proneness to mechanical compaction observed as reduced pore size for the high-TOC group or higher content of primary micropores associated with OM.

Several previous publications noted a similar observation that above a certain OM content, porosity either does not increase anymore with TOC or even declines. Milliken et al. (2013) observed that porosity values in the Marcellus Formation increase with OM content up to 5.6 wt % TOC; in samples above 5.6 wt% TOC there is no correlation between porosity and TOC. Additionally, samples above that TOC threshold showed a reduction in pore size. These samples were within the oil window and overmature, and the trend was interpreted as a result of higher hydrocarbon expulsion efficiency related to the increased OM connectivity in high-TOC samples, but it could also be lower resistance to compaction for high-TOC samples. Liu et al. (2017a) observed a decline in porosity with increasing TOC for two sample sets from the Silurian Longmaxi Formation above 4 and 6 wt% TOC. Knapp et al. (2020) observed in the Devonian Duvernay Formation a good correlation between helium porosity and TOC up to 5.6 wt% TOC and a decline in porosity in the sample with highest TOC (7.3 wt%). Chukwuma et al.

(2018), in the Permian Whitehill Formation, observed a weaker correlation between TOC and porosity in the samples with \geq 5.4 wt% TOC. Gao et al. (2022) in the Lower Paleozoic Wufeng-Longmaxi formations reported collapsing of larger organic pores in samples with TOC >5.5 wt %. Schieber (2010), based on scanning electron microscope observation of samples from several shale formations, stated that immature samples with high OM content (TOC > 10 wt%) have phyllosilicate pores filled with OM, and thus possibly lower porosity, while in samples with lower OM content (TOC < 7 wt%) a large portion of phyllosilicate pores was open. Kuila et al. (2014) reached similar conclusions for Silurian shales from the Baltic Basin and Paleozoic shales from North America, based on N₂ adsorption studies and SEM observations before and after OM removal. They found that immature mudstones and shales have a heterogeneous distribution of OM and clay aggregates, with pore structures dominated by clay-hosted micro- and meso-porosity, which may be open or partially filled by OM. Most of the above-cited studies indicate a threshold between 4 and 6 wt% TOC, above which increased compaction takes place. Lithological and mechanical rock parameters likely define the width and value of the OM content threshold.

5.2. Oil window (0.75 to 1.1 % VRE) maturity

With increasing maturity through the oil window, chemical compaction becomes increasingly more important, surpassing the importance of mechanical compaction above 70-80 °C (Mondol et al., 2008). Multiple processes, both inorganic (e.g., mineral dissolution and re-precipitation, crystallization of amorphous silica phases, clayrecrystallization and dehydration) and organic (organic acid, bitumen, and hydrocarbon generation with associated maceral conversion) take place, affecting porosity. At the immature and low-maturity stage, TPV values for low- and mid-TOC samples overlap. Moving into the oil window, the mid-TOC samples undergo a more significant decline in TPV values. The decrease in pore volume and surface area at the oil window stage has been observed before in OM-rich shales (Furmann et al., 2016; Han et al., 2017; Löhr et al., 2015; Mastalerz et al., 2018; Mastalerz et al., 2013; Wei et al., 2014) and artificially pyrolysed sample sets (Chen and Xiao, 2014; Guo et al., 2017; Wang et al., 2022). This decline has been related to pore filling and pore-throat plugging with bitumen (Löhr et al., 2015; Mastalerz et al., 2018; Mastalerz et al., 2013; Misch et al., 2019; Topór et al., 2017b; Wei et al., 2014; Wood et al., 2018; Wood et al., 2015). Microscopic observations confirm the gradual replacement of liptinite macerals with solid bitumen at the oil window stage (Fig. 2). TPV values through the oil window show an inverse relationship with TOC (Fig. 8C). This could be explained by the simple fact that the higher the OM content, the more bitumen is generated, filling more porosity and plugging more pore-throats. Interestingly, micropores behave differently, and the lowest micropore volume (Figs. 5A and 8D) is observed in the mid-TOC sample group, whereas low- and high-TOC samples have higher micropore volume and CO₂ SA. The low-TOC sample group produced less bitumen and showed less pore filling. The high-TOC sample group should have better expulsion through an interconnected OM network (Loucks et al., 2012; Loucks et al., 2009) than the mid-TOC group. Thus, more solid bitumen is retained in the mid-TOC group, preferentially plugging OM-associated micropores.

Secondary OM-hosted porosity should develop at the oil window stage. Its onset has been observed in previous studies (Cardott et al., 2015 at 0.9 %, Curtis et al., 2012 between 0.9 and 1.23 %, Loucks et al., 2012 at 0.6 %, Liu et al., 2021, at 1.05 %). As observed by İnan et al. (2018 and references therein) initially, the generated bitumen will be preferentially retained within kerogen; only above a certain threshold will it form separate particles. Eventually, the excess of bitumen is expelled from kerogen. The preferred location for the newly formed bitumen particles will be pressure shadows next to rigid minerals; thus, solid bitumen will be more prone to secondary porosity formation. The negative relationship between TOC and TPV in the oil window observed

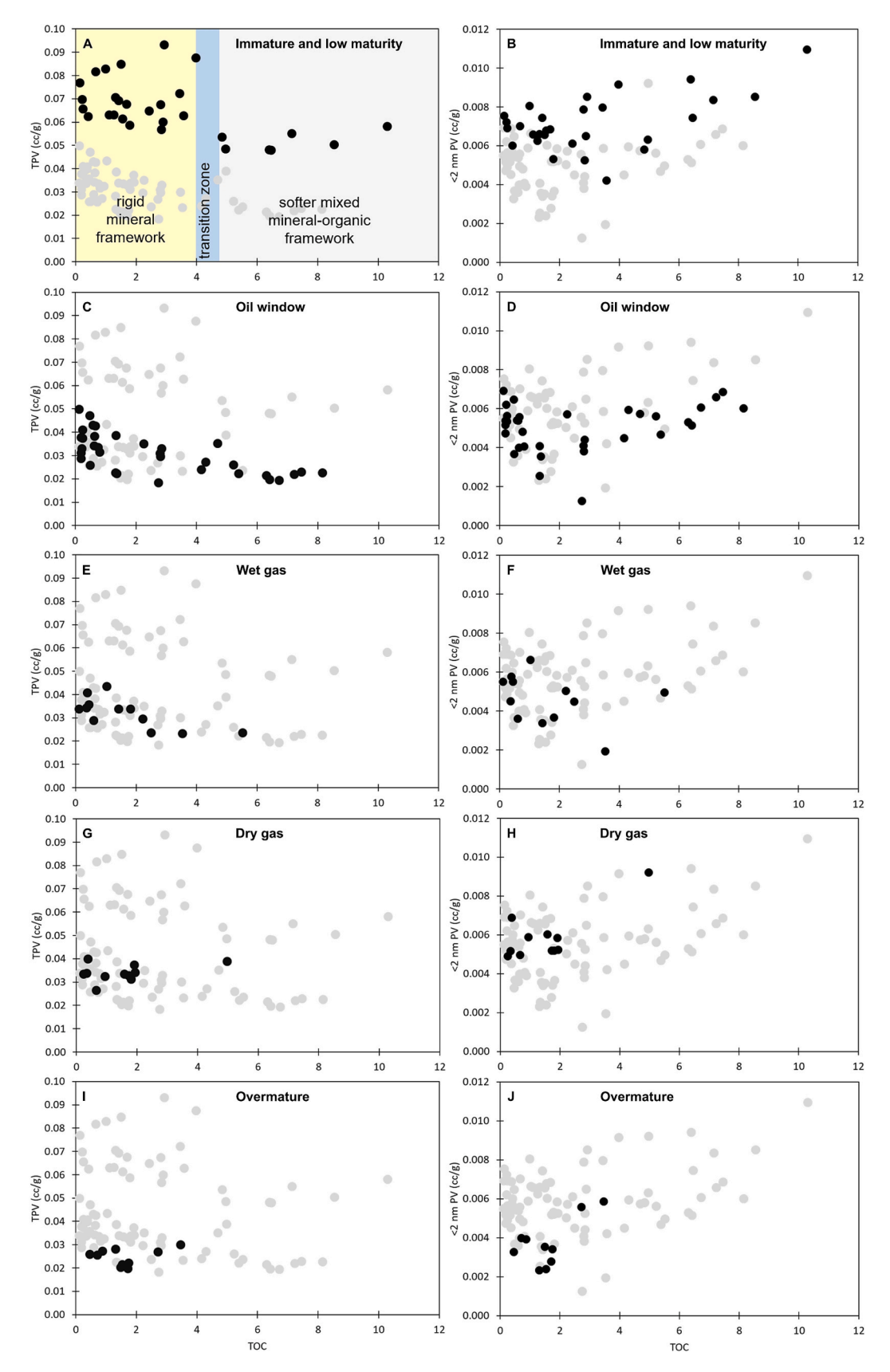


Fig. 8. Graphs showing relationships between TPV (A-E) and micropore volume (F-J) and TOC for the selected maturity stages. Black dots represent samples from the selected maturity stage, grey dots represent remaining samples.

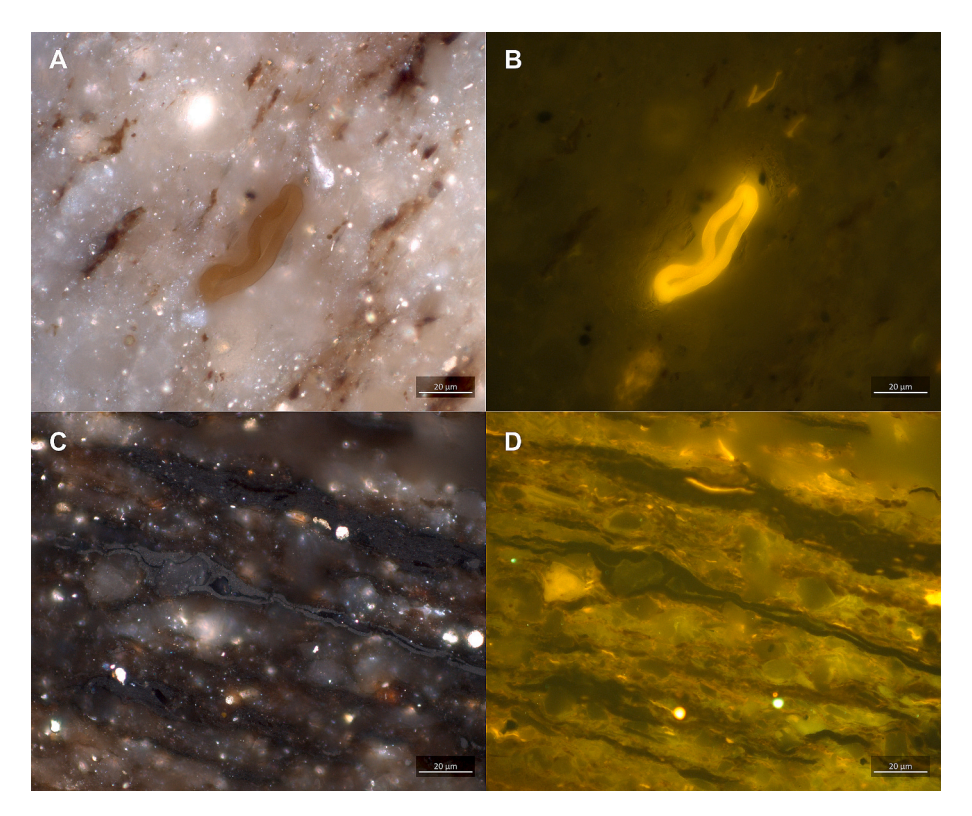


Fig. 9. Comparison of low-maturity dominantly mineral (A,B, low-TOC, sample BT9) and mixed organic-mineral (C,D, high-TOC, sample Bartoszyce IG-1) frameworks. Photomicrographs of A & C - reflected light, C & D - UV light; all in oil immersion.

in the studied samples indicates that pore filling and pore-throat plugging are more important than secondary porosity development. This is in contrast to other formations where a strong positive correlation between TOC and porosity has been documented at oil window maturity (e.g., Milliken et al., 2013).

5.3. Wet (1.1-1.4 % VRE) and dry (>1.4-2.0 % VRE) gas windows

At this maturity range, while all samples undergo diminishing compaction effects, best manifested in the low-TOC samples as a gradual porosity decline, organic-rich samples behave differently. The mid- and high-TOC samples reached minimum TPV at the end of the oil window, and through the wet gas window, there is an increase in TPV that continues through the dry gas window. The trend is visible not only for TPV, but also for micro-, meso-, and macropores, BET SA, and CO₂ SA (Figs. 4, 5, 6, 7). While at the wet gas window, a slight negative correlation still exists between TOC and porosity (Fig. 8E,F), at the dry gas stage, the negative correlation exists for microporosity (Fig. 8G,H). The increase in porosity could be associated with developing secondary OM-hosted porosity or pore-throats unplugging, which will be further discussed in Section 5.5.

5.4. Overmature samples

Further maturity increase beyond the gas window in studied samples reveals a very gentle decline in TPV, BET SA, CO_2 SA, micropore, and mesopore volumes (Figs. 4, 5, 6, 7). Only macropore volume is an exception, displaying roughly constant values for all sample groups. Micropore volume (Fig. 5) for overmature high-TOC samples shows much higher values than for two other sample groups, again confirming the affinity between microporosity and OM. A positive correlation also exists between TOC and micropore volume (Fig. 8J).

At the overmature stage, the hydrocarbon generation potential is

almost exhausted; thus, secondary OM porosity generation is unlikely. The correlations between TOC and both TPV and micropore volume are similar to those in the dry gas stage, but the pore volumes are lower. An increase in overburden pressure between the dry gas window and the overmature stage leads to further compaction. At this stage, OM is becoming mechanically stiffer than clay minerals. Wang et al. (2022) reports Young's modulus values for overmature OM (2.1 to 4.5 EasyRo %) to be between 5.59 and 9.71 GPa. These values are comparable to or sometimes greater than Young's modulus for different clay minerals: kaolinite 2.59 GPa (Pal-Bathija et al., 2008), 1.3 GPa for fresh rising to 6.9 GPa upon heating (Mikowski et al., 2007); 5 to 8 GPa for kaoliniteillite mixtures (Húlan and Štubňa, 2020); montmorillonite 7.26 GPa (Pal-Bathija et al., 2008); and 6.2 GPa for dickite (Prasad et al., 2002). Thus, even if compaction leads to a decrease in pore volumes, it no longer preferentially affects the OM. The continuing correlation from the dry gas window between micropores and TOC suggests that OM (with its hosted porosity) is no longer weaker than the surrounding mineral matrix and resistant to preferential compaction. The fact that micropore volume shows correlation with TOC and meso- and macropores don't, may suggest that micropores are more resistant to compaction than meso- and macropores and/or that the latter two are compacted to form micropores.

5.5. Porosity decline mechanisms: pore-throat plugging vs pore filling

The decrease of TPV, micropore volume, as well as BET and $\rm CO_2$ surface areas through the oil window is associated with kerogen transformation, hydrocarbon/bitumen generation, and related pore-throat plugging and/or pore filling. This is documented by the difference in adsorption parameters (pore volumes and surface areas) between midand high-TOC, and low-TOC sample groups. The mid-TOC samples between 0.9 and 1.1 % VRE have an average TOC content of 2.3 wt%, which, based on the oil window type II kerogen density of 1.28 g/cc (Stankiewicz et al., 2015), can be translated into 5.6 vol% of OM

(assuming 0.8 as the carbon weight fraction in OM). At 1.0 % VRE, the difference in TPV between low- and mid-TOC groups is around 0.02 cc/ g. Assuming 2.5 g/cc as the average shale density, a 0.02 g/cc difference in TPV translates to a 5 % decrease in porosity between the low- and mid-TOC sample groups. Thus, the volume of OM (5.6 %) is just slightly more than the volume of porosity loss due to bitumen pore-throat plugging or pore filling. If pore filling were the dominant mechanism for porosity decrease, then either OM would have to increase in volume by 90 % (due to chemical conversion to liquid hydrocarbons), or 90 % of OM would have to become mobile, migrate within the shale, and fill the pores. The third option would be a combination of the two abovementioned processes. In any case, these are impossible or highly unlikely scenarios. Alternatively, porosity decrease can be explained more easily by a slight increase in OM volume due to bitumen generation, migration within shale, and pore-throat plugging. This suggests that pore-throat plugging rather than pore filling is the dominant mechanism responsible for measured porosity decline within the oil window. Porethroat plugging prevents N₂ and CO₂ adsorbants from accessing pores, thus adsorption measured porosity can be described as the accessible porosity. Pores that are not completely filled, but rendered inaccessible due to plugging, will contribute to the total porosity, but not to the accessible porosity. Thus the total porosity (not measured in this study), likely experiences lower decline than accessible porosity at the oil window stage. As a result the difference between effective and total porosity should increase due to pore-throat plugging. That difference can also increase with increasing TOC, with more pores plugged and rendered non-accessible in high TOC samples.

Furthermore, a maturity increase from 1.0 % VRE through the wet and dry gas windows (to 2.0 % VRE) results in a porosity increase of 2.5 % (0.01 g/cc) for the mid-TOC group. A model presented by (Modica and Lapierre, 2012, their Fig. 9) indicates that at 1.0 % vitrinite reflectance, 90 % of OM secondary porosity is already generated. Thus, further increase in maturity can generate a maximum of 0.35 % additional secondary porosity (for 4.0 % initial TOC pathway in their Fig. 9). This indicates that in the observable 2.5 % porosity increase for the mid-TOC group from the oil window to the dry gas window, a maximum of 0.35 % can be the result of secondary porosity generation in bitumenfilled pores. The remaining 2.15 % porosity increase is the result of pore-throat unplugging. Caution, however, needs to be taken with the above approach, as different studies present development of secondary porosity at slightly different maturity ranges (see Katz and Arango, 2018, and references therein) with potential secondary porosity development even past 2.0 % Ro (Chen and Xiao, 2014; Curtis et al., 2012; Luo and Zhong, 2020).

Analogously, for the high-TOC group, the porosity increase from 1.0 to $2.0\,\%$ VRE is roughly $3.75\,\%$ ($0.15\,\text{cc/g}$). Assuming $8.0\,\%$ as the initial average TOC for this group and scaling Modica and Lapierre's (2012) model, $0.7\,\%$ of the porosity increase can be attributed to the generation of secondary OM-hosted porosity, leaving a $3.05\,\%$ porosity increase to pore-throat unplugging. In both cases, in mid- and high-TOC groups, the majority of porosity increase is related to pore-throat unplugging, but the fraction of porosity increase related to unplugging decreases with increasing TOC ($0.86\,$ for the mid- and $0.81\,$ for the high-TOC group), indicating more pore filling with increasing OM content. Pore-throat unplugging does not mean complete removal of bitumen-plugging pores. It is more likely related to the generation of secondary porosity within the bitumen plug, making it porous and permeable enough for CO2 and N2 adsorbants to access the previously blocked pore.

The dominance of coupled pore-throat plugging and unplugging (vs. pore filling and significant secondary porosity generation) as a potential mechanism of oil window porosity decrease and gas window porosity increase is corroborated by observations of poor secondary porosity development in the same Silurian shales from the Baltic Basin made by Milliken et al. (2018). In different shales, Lomando (1992), based on the observations that solid bitumen presence leads to a significant reduction in permeability and only "some porosity reduction," concluded the

blockage of pore-throats to be the principal cause. Fan et al. (2024), performing artificial maturation experiments on shales from the Sinian Xiamaling and Permian Shanxi Formations, calculated that micropore volume increase during gas generation is primarily due to the opening of previously existing pores rather than self-generated new pores. Still, for pores bigger than 2 nm, self-generation contributed more to pore volume increase than the release of previously blocked pores.

5.6. Maceral composition effect on reservoir properties

Although fossils of terrestrial vascular plants from the early Silurian have not been found so far, the geochemical signatures suggest that vascular plants have already colonized the land (Yuan et al., 2023). The lack of fossils may indicate either no colonization or only localized one. No terrestrial-derived macerals from vitrinite and inertinite groups were observed in the studied sample set. As terrestrial OM has a different chemical composition and potential for secondary porosity development than marine OM, its input would introduce another factor to be considered. Without the presence of terrestrial OM, the changes in OM maceral composition are mainly related to thermal maturity and not to the input of terrigenous material.

OM in immature and low-maturity samples is dominated by macerals from the liptinite group, which convert to solid bitumen with increasing maturity. Solid bitumen is widely known for developing extensive secondary porosity (Cardott et al., 2015; Delle Piane et al., 2022; Liu et al., 2017b; Suárez-Ruiz et al., 2016; Wood et al., 2015; Zhang et al., 2020). The remaining OM comprises zooclasts, mostly graptolite (up to 20 % by volume) with trace amounts of chitinozoa and acritarchs. There is ongoing discussion about the secondary porosity development potential in graptolites, with the majority of studies observing little to no secondary porosity (e.g., Delle Piane et al., 2022; Li et al., 2018b; Teng et al., 2022; Zhang et al., 2020), whereas other studies observe porosity development (Ma et al., 2016; Xu et al., 2020). The maceral composition of the studied early Silurian shale can be compared with the Wufeng-Longmaxi Shale (upper Ordovician-early Silurian), where the graptolite content can be similar (Teng et al., 2022) or higher (Luo et al., 2016). The porosity in the Wufeng-Longmaxi Shale, at least in some cases (Ma et al., 2016), strongly correlates with TOC, suggesting the importance of OM-hosted porosity for reservoir storage. With high graptolite content, the Wufeng-Longmaxi Shale is still one of the world's most successful shale gas plays with 20 billion m³ gas production in 2020 (Nie et al., 2021). Based on this comparison, the authors conclude that the graptolite content, in the amount up to 20 % by volume as observed in the studied samples, should not be responsible for the low gas production in the studied formation.

5.7. Implications for reservoir quality

The majority of gas shale studies show a positive correlation between TOC and porosity (Jarvie, 2012b; Milliken et al., 2013; Milliken et al., 2012; Passey et al., 2010; Ross and Bustin, 2009; Wang et al., 2024, among others), indicating OM-related (hosted) porosity plays an important role in gas shale reservoirs. In the case of studied Silurian shales from the Baltic Basin, a negative correlation exists between TOC and TPV for the samples of the wet gas maturity and no correlation for the samples of the dry gas and overmature stages. For the micropore volume, no correlation was found with TOC at the wet gas stage, and a positive, although weak, correlation at the dry gas and overmature stage. This suggests poor development of secondary OM porosity within the studied samples.

Clay content in studied shales is, on average, around 50 % by volume (Topór et al., 2017a). Similar clay content was reported by other authors for this formation (Lutyński et al., 2017; Milliken et al., 2012; Słomski et al., 2021). This is higher than in the majority of producing gas shale reservoirs in the United States (Chermak and Schreiber, 2014; Fishman et al., 2015; Hupp and Donovan, 2018; Sahoo et al., 2013), Canada

(Knapp et al., 2020) or China (Wang et al., 2019). Clay and OM are mechanically weak rock constituents. Their content correlates inversely with shale hardness (Kumar et al., 2012). They comprise the majority of studied rocks by volume, creating a non-rigid mineral or mixed mineralorganic framework. This has two implications for reservoir quality: first, the lack of rigid framework enhanced hydrocarbon expulsion in the past and reduced the hydrocarbons retained within the shale; and second, the lack of pressure shadows provided by rigid mineral framework impaired secondary porosity development within OM. Milliken et al. (2018) studied grain assemblages in the same shale horizon and observed rigid silt particles floating within clay dominated matrix. Silt content was too low in most samples to provide a mechanically rigid framework. As a result, they observed little secondary OM-hosted porosity using electron microscopy. As observed by Dong et al. (2017) and Gao et al. (2022), detrital quartz has little effect on porosity preservation, whereas authigenic quartz cementation positively correlates with brittleness, forming a rigid mineral framework and enhancing primary porosity preservation. As reported by Milliken et al. (2018), who observed quartz cementation only in 3 out of 41 studied samples, shales from the Baltic Basin are characterized by relatively little quartz cement.

The influence of rock framework physical properties on the preservation of primary and development of secondary porosity has recently attracted more attention (Dong et al., 2019; Dong and Harris, 2020; Fishman et al., 2012; Gao et al., 2023; Gao et al., 2022; Knapp et al., 2020). Fishman et al. (2012) studied the porosity of the organic-rich Kimmeridge Clay Formation, where mechanically weak rock constituents often dominate the rock fabric, like in our samples. Similarly, they observed little OM-hosted secondary porosity, suggesting that if such porosity developed, it was not preserved in a ductile environment.

The lack of positive TOC-TPV correlation documented in this study indicates the dominance of inorganic porosity and little contribution from organic porosity. Mechanically weak rock framework not only led to the greater porosity collapse in high-TOC samples as observed in immature and low maturity samples, but it was also ineffective in providing pressure shadows for significant development of OM-hosted porosity.

6. Summary and conclusions

Our results show the influence of varying OM content on porosity evolution in mudstones. Although multiple other processes and factors affect porosity, introducing scatter to the measured data, a large number of samples (96) allows us to observe porosity evolution trends and draw the following conclusions:

- Porosity in the studied organic-rich shales through most of the thermal evolution (immature, oil, and wet gas windows) is lower than in organic-lean shale samples. Only in dry gas and overmature samples is the porosity equal to or higher than in the organic-lean samples.
- 2. High OM content (here, above the 4.0–4.8 wt% TOC threshold; mostly 4–6 wt% TOC in other studies) disrupts the mineral framework, leading to a mixed organic-mineral framework. Due to the weak mechanical stiffness of OM, the mixed framework is more prone to compaction. This is observable as lower porosity in high-OM-content samples for immature and low-maturity samples.
- 3. Pore-throat plugging, rather than pore filling, is the dominant mechanism for porosity decrease observed during the oil window stage. Unplugging of pore-throats during wet and dry gas stages is the dominant mechanism for increasing porosity. With increasing OM content, the pore filling mechanism relatively increases but does not surpass pore-throat plugging in importance.
- 4. The absence of or weak correlation between TOC and TPV or microporosity suggests poor development of secondary OM porosity within the studied samples. Mineral-associated porosity dominates. High clay content (50 % by volume) fails to provide the rigid

framework and pressure shadows necessary for secondary OM porosity development.

Author statement

The article is the authors' original work, hasn't received prior publication and isn't under consideration for publication elsewhere.

All authors have seen and approved the final version of the manuscript being submitted.

Funding sources

This study was funded by the National Science Centre, Poland, project 2019/35/B/ST10/00385.

CRediT authorship contribution statement

Grzegorz P. Lis: Conceptualization, Funding acquisition, Investigation, Writing – original draft, Supervision. **Tomasz Topór:** Resources, Investigation, Writing – original draft. **Maria Mastalerz:** Investigation, Writing – original draft.

Declaration of competing interest

The authors declare the following financial interests/personal relationships which may be considered as potential competing interests:

Grzegorz P. Lis reports financial support was provided by National Science Centre Poland. If there are other authors, they declare that they have no known competing financial interests or personal relationships that could have appeared to influence the work reported in this paper.

Data availability

Data will be made available on request.

References

- ASTM, 2015. D2797 Standard practice for preparing coal samples for microscopical analysis by reflected light. In: Backeberg, P.A., Iacoviel, N.R. (Eds.), Petroleum Products, Lubricants, and Fossil Fuels; Gaseous Fuels; Coal and Coke, sec. 5, v. 05.06. ASTM International, West Conshohocken.
- Bjørlykke, K., Høeg, K., 1997. Effects of burial diagenesis on stresses, compaction and fluid flow in sedimentary basins. Mar. Pet. Geol. 14, 267–276. https://doi.org/ 10.1016/S0264-8172(96)00051-7.
- Bruant Jr., R.G., Celia, M.A., Guswa, A.J., Peters, C.A., 2002. Peer reviewed: safe storage of CO2 in deep saline aquifiers. Environ. Sci. Technol. 36, 240A–245A. https://doi. org/10.1021/es0223325.
- Bustin, R.M., Bustin, A.M.M., Cui, X., Ross, D.J.K., Pathi, V.S.M., 2008. Impact of shale properties on pore structure and storage characteristics. In: All Days. Presented at the SPE Shale Gas Production Conference. SPE, Fort Worth, Texas, USA. https://doi.org/10.2118/119892-MS p. SPE-119892-MS.
- Cardott, B.J., Landis, C.R., Curtis, M.E., 2015. Post-oil solid bitumen network in the Woodford Shale, USA — a potential primary migration pathway. Int. J. Coal Geol. 139, 106–113. https://doi.org/10.1016/j.coal.2014.08.012.
- Chalmers, G.R.L., Bustin, R.M., 2007. The organic matter distribution and methane capacity of the Lower Cretaceous strata of Northeastern British Columbia, Canada. Int. J. Coal Geol. 70, 223–239. https://doi.org/10.1016/j.coal.2006.05.001.
- Chen, J., Xiao, X., 2014. Evolution of nanoporosity in organic-rich shales during thermal maturation. Fuel 129. 173–181. https://doi.org/10.1016/j.fuel.2014.03.058.
- Chermak, J.A., Schreiber, M.E., 2014. Mineralogy and trace element geochemistry of gas shales in the United States: environmental implications. Int. J. Coal Geol. 126, 32–44. https://doi.org/10.1016/j.coal.2013.12.005.
- Chukwuma, K., Bordy, E.M., Coetzer, A., 2018. Evolution of porosity and pore geometry in the Permian Whitehill Formation of South Africa – a FE-SEM image analysis study. Mar. Pet. Geol. 91, 262–278. https://doi.org/10.1016/j.marpetgeo.2017.12.026.
- Clarkson, C.R., Solano, N., Bustin, R.M., Bustin, A.M.M., Chalmers, G.R.L., He, L., Melnichenko, Y.B., Radliński, A.P., Blach, T.P., 2013. Pore structure characterization of North American shale gas reservoirs using USANS/SANS, gas adsorption, and mercury intrusion. Fuel 103, 606–616. https://doi.org/10.1016/j.fuel.2012.06.119.
- Curtis, M.E., Cardott, B.J., Sondergeld, C.H., Rai, C.S., 2012. Development of organic porosity in the Woodford Shale with increasing thermal maturity. Int. J. Coal Geol. 103, 26–31. https://doi.org/10.1016/j.coal.2012.08.004.
- Delle Piane, C., Ansari, H., Li, Z., Mata, J., Rickard, W., Pini, R., Dewhurst, D.N., Sherwood, N., 2022. Influence of organic matter type on porosity development in the Wufeng-Longmaxi Shale: a combined microscopy, neutron scattering and

- physisorption approach. Int. J. Coal Geol. 249, 103880. https://doi.org/10.1016/j.
- Derkowski, A., Marynowski, L., 2016. Reactivation of cation exchange properties in black shales. Int. J. Coal Geol. 158, 65–77. https://doi.org/10.1016/j. coal.2016.03.002.
- Dong, T., Harris, N.B., 2020. The effect of thermal maturity on porosity development in the Upper Devonian –lower Mississippian Woodford Shale, Permian Basin, US: insights into the role of silica nanospheres and microcrystalline quartz on porosity preservation. Int. J. Coal Geol. 217, 103346. https://doi.org/10.1016/j. coal.2019.103346.
- Dong, T., Harris, N.B., Ayranci, K., Yang, S., 2017. The impact of rock composition on geomechanical properties of a shale formation: Middle and Upper Devonian Horn River Group shale, Northeast British Columbia, Canada. Bulletin 101, 177–204. https://doi.org/10.1306/07251615199.
- Dong, T., He, S., Chen, M., Hou, Y., Guo, X., Wei, C., Han, Y., Yang, R., 2019. Quartz types and origins in the paleozoic Wufeng-Longmaxi Formations, Eastern Sichuan Basin, China: implications for porosity preservation in shale reservoirs. Mar. Pet. Geol. 106, 62–73. https://doi.org/10.1016/j.marpetgeo.2019.05.002.
- Fan, Q., Cheng, P., Gai, H., Yu, Z., Meng, G., Xiao, X., 2024. Effects of post-oil bitumen on the nanopore development of shales: new insights from a stepwise thermal simulation experiment on small shale plug samples. Mar. Pet. Geol. 168, 107038. https://doi.org/10.1016/j.marpetgeo.2024.107038.
- Fishman, N.S., Hackley, P.C., Lowers, H.A., Hill, R.J., Egenhoff, S.O., Eberl, D.D., Blum, A.E., 2012. The nature of porosity in organic-rich mudstones of the Upper Jurassic Kimmeridge Clay Formation, North Sea, offshore United Kingdom. Int. J. Coal Geol. 103, 32–50. https://doi.org/10.1016/j.coal.2012.07.012.
- Fishman, N.S., Egenhoff, S.O., Boehlke, A.R., Lowers, H.A., 2015. Petrology and diagenetic history of the upper shale member of the Late Devonian–Early Mississippian Bakken Formation, Williston Basin, North Dakota. In: Geological Society of America Special Papers. Geological Society of America, pp. 125–151. https://doi.org/10.1130/2015.2515(07.
- Furmann, A., Mastalerz, M., Bish, D., Schimmelmann, A., Pedersen, P.K., 2016. Porosity and pore size distribution in mudrocks from the Belle Fourche and Second White Specks Formations in Alberta, Canada. Bulletin 100, 1265–1288. https://doi.org/ 10.1306/02191615118.
- Gao, P., Xiao, X., Hu, D., Lash, G.G., Liu, R., Cai, Y., Wang, Z., Zhang, B., Yuan, T., Liu, S., 2022. Effect of silica diagenesis on porosity evolution of deep gas shale reservoir of the lower Paleozoic Wufeng-Longmaxi formations, Sichuan Basin. Mar. Pet. Geol. 145, 105873. https://doi.org/10.1016/j.marpetgeo.2022.105873.
- Gao, P., Xiao, X., Meng, G., Lash, G.G., Li, S., Han, Y., 2023. Quartz types and origins of the Upper Permian Dalong Formation shale of the Sichuan Basin: implications for pore preservation in deep shale reservoirs. Mar. Pet. Geol. 156, 106461. https://doi. org/10.1016/j.maruetgeo.2023.106461.
- Grathoff, G.H., Peltz, M., Enzmann, F., Kaufhold, S., 2016. Porosity and permeability determination of organic-rich Posidonia shales based on 3-D analyses by FIB-SEM microscopy. Solid Earth 7, 1145–1156. https://doi.org/10.5194/se-7-1145-2016.
- Gregg, S.J., Sing, S.W., 1982. Adsorption, Surface Area, and Porosity. Academic Press, New York.
- Guo, H., Jia, W., Peng, P., Zeng, J., He, R., 2017. Evolution of organic matter and nanometer-scale pores in an artificially matured shale undergoing two distinct types of pyrolysis: a study of the Yanchang Shale with Type II kerogen. Org. Geochem. 105, 56–66. https://doi.org/10.1016/j.orggeochem.2017.01.004.
- Hackley, P.C., Valentine, B.J., Hatcherian, J.J., 2018. On the petrographic distinction of bituminite from solid bitumen in immature to early mature source rocks. Int. J. Coal Geol. 196, 232–245. https://doi.org/10.1016/j.coal.2018.06.004.
- Han, Y., Horsfield, B., Wirth, R., Mahlstedt, N., Bernard, S., 2017. Oil retention and porosity evolution in organic-rich shales. Bulletin 101, 807–827. https://doi.org/ 10.1306/09221616069
- Hendel, J., Kuczyński, S., Sikora, P., 2015. Shale gas revolution in Poland challenges with replication of the US success. In: Recent Advances in Environmental and Earth Sciences and Economics. Proceeding of the 2015 International Conference on Energy, Environment, Development and Economics, Zakynthos Island, Greece (2015), pp. 22–31.
- Húlan, T., Štubňa, I., 2020. Young's modulus of kaolinite-illite mixtures during firing. Appl. Clay Sci. 190, 105584. https://doi.org/10.1016/j.clay.2020.105584.
- Hupp, B.N., Donovan, J.J., 2018. Quantitative mineralogy for facies definition in the Marcellus Shale (Appalachian Basin, USA) using XRD-XRF integration. Sediment. Geol. 371, 16–31. https://doi.org/10.1016/j.sedgeo.2018.04.007.
- Inan, S., Al Badairy, H., İnan, T., Al Zahrani, A., 2018. Formation and occurrence of organic matter-hosted porosity in shales. Int. J. Coal Geol. 199, 39–51. https://doi. org/10.1016/j.coal.2018.09.021.
- Jacob, H., 1989. Classification, structure, genesis and practical importance of natural solid oil bitumen ("migrabitumen"). Int. J. Coal Geol. 11, 65–79. https://doi.org/ 10.1016/0166-5162(89)90113-4.
- Jarvie, D.M., 2012a. Shale resource systems for oil and gas part 2 shale-oil resource systems. In: Shale Reservoirs—Giant Resources for the 21st Century. American Association of Petroleum Geologists. https://doi.org/10.1306/13321447M973489.
- Jarvie, D.M., 2012b. Shale resource systems for oil and gas part 1—shale-gas resource systems. In: Shale Reservoirs—Giant Resources for the 21st Century. American Association of Petroleum Geologists. https://doi.org/10.1306/13321446M973489.
- Jarvie, D.M., Hill, R.J., Ruble, T.E., Pollastro, R.M., 2007. Unconventional shale-gas systems: the Mississippian Barnett Shale of north-Central Texas as one model for thermogenic shale-gas assessment. Bulletin 91, 475–499. https://doi.org/10.1306/ 12190606068.
- Karnkowski, P.H., 2007. Petroleum provinces in Poland. Prz. Geol. 55, 1.

- Katz, B.J., Arango, I., 2018. Organic porosity: a geochemist's view of the current state of understanding. Org. Geochem. 123, 1–16. https://doi.org/10.1016/j. orggeochem.2018.05.015.
- Knapp, L.J., Ardakani, O.H., Uchida, S., Nanjo, T., Otomo, C., Hattori, T., 2020. The influence of rigid matrix minerals on organic porosity and pore size in shale reservoirs: Upper Devonian Duvernay Formation, Alberta, Canada. Int. J. Coal Geol. 227, 103525. https://doi.org/10.1016/j.coal.2020.103525.
- Kuila, U., McCarty, D.K., Derkowski, A., Fischer, T.B., Topór, T., Prasad, M., 2014. Nano-scale texture and porosity of organic matter and clay minerals in organic-rich mudrocks. Fuel 135, 359–373. https://doi.org/10.1016/j.fuel.2014.06.036.
- Kumar, V., Sondergeld, C.H., Rai, C.S., 2012. Nano to macro mechanical characterization of shale. In: All Days. Presented at the SPE Annual Technical Conference and Exhibition. SPE, San Antonio, Texas, USA. https://doi.org/10.2118/159804-MS p. SPE-159804-MS.
- Li, C., Ostadhassan, M., Gentzis, T., Kong, L., Carvajal-Ortiz, H., Bubach, B., 2018a. Nanomechanical characterization of organic matter in the Bakken formation by microscopy-based method. Mar. Pet. Geol. 96, 128–138. https://doi.org/10.1016/j. marpetgeo.2018.05.019.
- Li, Y., Schieber, J., Fan, T., Wei, X., 2018b. Pore characterization and shale facies analysis of the Ordovician-Silurian transition of northern Guizhou, South China: the controls of shale facies on pore distribution. Mar. Pet. Geol. 92, 697–718. https:// doi.org/10.1016/j.marpetgeo.2017.12.001.
- Li, C., Ostadhassan, M., Abarghani, A., Fogden, A., Kong, L., 2019. Multi-scale evaluation of mechanical properties of the Bakken shale. J. Mater. Sci. 54, 2133–2151. https:// doi.org/10.1007/s10853-018-2946-4.
- Liu, W., Liu, J., Cai, M., Luo, C., Shi, X., Zhang, J., 2017a. Pore evolution characteristic of shale in the Longmaxi Formation, Sichuan Basin. Pet. Res. 2, 291–300. https://doi. org/10.1016/j.ptlrs.2017.03.003.
- Liu, B., Schieber, J., Mastalerz, M., 2017b. Combined SEM and reflected light petrography of organic matter in the New Albany Shale (Devonian-Mississippian) in the Illinois Basin: a perspective on organic pore development with thermal maturation. Int. J. Coal Geol. 184, 57–72. https://doi.org/10.1016/j. coal.2017.11.002.
- Liu, B., Schieber, J., Mastalerz, M., 2019. Petrographic and micro-FTIR study of organic matter in the Upper Devonian New Albany shale during thermal maturation: implications for Kerogen transformation. In: Camp, W.K., Fishman, N.S., Hackley, P. C., Macquaker, J.H.S., Milliken, K.L., Taylor, K.G. (Eds.), Memoir 120: Mudstone Diagenesis: Research Perspectives for Shale Hydrocarbon Reservoirs, Seals, and Source Rocks. AAPG, pp. 165–188. https://doi.org/10.1306/13672216M1213380.
- Liu, B., Teng, J., Mastalerz, M., Schieber, J., Schimmelmann, A., Bish, D., 2021. Compositional control on shale pore structure characteristics across a maturation gradient: insights from the Devonian New Albany shale and Marcellus shale in the Eastern United States. Energy Fuel 35, 7913–7929. https://doi.org/10.1021/acs. energyfuels.1c00526.
- Löhr, S.C., Baruch, E.T., Hall, P.A., Kennedy, M.J., 2015. Is organic pore development in gas shales influenced by the primary porosity and structure of thermally immature organic matter? Org. Geochem. 87, 119–132. https://doi.org/10.1016/j.
- Lomando, A.J., 1992. The influence of solid reservoir bitumen on reservoir quality (1). Bulletin 76. https://doi.org/10.1306/BDFF8984-1718-11D7-8645000102C1865D.
- Loucks, R.G., Reed, R.M., Ruppel, S.C., Jarvie, D.M., 2009. Morphology, genesis, and distribution of nanometer-scale pores in siliceous mudstones of the Mississippian Barnett Shale. J. Sediment. Res. 79, 848–861. https://doi.org/10.2110/ isr.2009.092.
- Loucks, R.G., Reed, R.M., Ruppel, S.C., Hammes, U., 2012. Spectrum of pore types and networks in mudrocks and a descriptive classification for matrix-related mudrock pores. AAPG Bull. 96, 1071–1098. https://doi.org/10.1306/08171111061.
- Luo, P., Zhong, N., 2020. The role of residual bitumen on the pore structure of organic-rich shales from low to over mature: insight from shale and coal samples after the hydrous pyrolysis. Int. J. Coal Geol. 226, 103515. https://doi.org/10.1016/j.coal.2020.103515.
- Luo, Q., Zhong, N., Dai, N., Zhang, W., 2016. Graptolite-derived organic matter in the Wufeng–Longmaxi Formations (Upper Ordovician–Lower Silurian) of southeastern Chongqing, China: implications for gas shale evaluation. Int. J. Coal Geol. 153, 87–98. https://doi.org/10.1016/j.coal.2015.11.014.
- Lutyński, M., Waszczuk, P., Slomski, P., Szczepański, J., 2017. CO 2 sorption of Pomeranian gas bearing shales the effect of clay minerals. Energy Procedia 125, 457–466. https://doi.org/10.1016/j.egypro.2017.08.153.
- Ma, Y., Zhong, N., Cheng, L., Pan, Z., Dai, N., Zhang, Y., Yang, L., 2016. Pore structure of the graptolite-derived OM in the Longmaxi Shale, southeastern Upper Yangtze Region, China. Mar. Pet. Geol. 72, 1–11. https://doi.org/10.1016/j. marpetgeo.2016.01.009.
- Mastalerz, M., Schimmelmann, A., Drobniak, A., Chen, Y., 2013. Porosity of Devonian and Mississippian New Albany Shale across a maturation gradient: insights from organic petrology, gas adsorption, and mercury intrusion. Bulletin 97, 1621–1643. https://doi.org/10.1306/04011312194.
- Mastalerz, M., Drobniak, A., Stankiewicz, A.B., 2018. Origin, properties, and implications of solid bitumen in source-rock reservoirs: a review. Int. J. Coal Geol. 195, 14–36. https://doi.org/10.1016/j.coal.2018.05.013.
- Mazur, S., Mikolajczak, M., Krzywiec, P., Malinowski, M., Buffenmyer, V., Lewandowski, M., 2015. Is the Teisseyre-Tornquist Zone an ancient plate boundary of Baltica? Tectonics 34, 2465–2477. https://doi.org/10.1002/2015TC003934.
- Mikowski, A., Soares, P., Wypych, F., Gardolinski, J.E.F.C., Lepienski, C., 2007.
 Mechanical properties of kaolinite 'macro-crystals'. Philos. Mag. 87, 4445–4459.
 https://doi.org/10.1080/14786430701550394.

- Milliken, K.L., Olson, T., 2017. Silica diagenesis, porosity evolution, and mechanical behavior in siliceous mudstones, Mowry Shale (cretaceous), Rocky Mountains, U.S. A. J. Sediment. Res. 87, 366–387. https://doi.org/10.2110/jsr.2017.24.
- Milliken, K.L., Esch, W.L., Reed, R.M., Zhang, T., 2012. Grain assemblages and strong diagenetic overprinting in siliceous mudrocks, Barnett Shale (Mississippian), Fort Worth Basin, Texas. Bulletin 96, 1553–1578. https://doi.org/10.1306/ 120111111129.
- Milliken, K.L., Rudnicki, M., Awwiller, D.N., Zhang, T., 2013. Organic matter-hosted pore system, Marcellus Formation (Devonian), Pennsylvania. Bulletin 97, 177–200. https://doi.org/10.1306/07231212048.
- Milliken, K.L., McCarty, D.K., Derkowski, A., 2018. Grain assemblages and diagenesis in the tarl-dominated lower Silurian mudrock succession of the western margin of the east European craton in Poland and Lithuania. Sediment. Geol. 374, 115–133. https://doi.org/10.1016/j.sedgeo.2018.07.011.
- Misch, D., Gross, D., Hawranek, G., Horsfield, B., Klaver, J., Mendez-Martin, F., Urai, J. L., Vranjes-Wessely, S., Sachsenhofer, R.F., Schmatz, J., Li, J., Zou, C., 2019. Solid bitumen in shales: petrographic characteristics and implications for reservoir characterization. Int. J. Coal Geol. 205, 14–31. https://doi.org/10.1016/j.coal.2019.02.012.
- Modica, C.J., Lapierre, S.G., 2012. Estimation of kerogen porosity in source rocks as a function of thermal transformation: example from the Mowry Shale in the Powder River Basin of Wyoming. Bulletin 96, 87–108. https://doi.org/10.1306/04111110201
- Modliński, Z., Szymański, B., 2001. The Silurian of the Nida, Holy Cross Mts. and Radom areas, Poland a review. Geol. Q. 45, 435–454.
- Modliński, Z., Jacyna, J., Kanev, S., Khubidikov, A., Laskova, L., Laskovas, J., Lendzion, K., Mikazane, I., Pomeranceva, R., 1999. Palaeotectonic evolution of the Baltic Syneclise during the early Palaeozoic as documented by palaeothickness maps. Kwartalnik Geol. 43, 285–296.
- Mondol, N.H., Bjørlykke, K., Jahren, J., Høeg, K., 2007. Experimental mechanical compaction of clay mineral aggregates—changes in physical properties of mudstones during burial. Mar. Pet. Geol. 24, 289–311. https://doi.org/10.1016/j. marpetgeo.2007.03.006.
- Mondol, N.H., Fawad, M., Jahren, J., Bjørlykke, K., 2008. Synthetic mudstone compaction trends and their use in pore pressure prediction. First Break 26. https:// doi.org/10.3997/1365-2397.2008018.
- Nawrocki, J., Poprawa, P., 2006. Development of trans-European suture zone in Poland: from Ediacaran rifting to early Palaeozoic accretion. Geol. Q. 50, 59–76.
- Nie, H., Chen, Q., Zhang, G., Sun, C., Wang, P., Lu, Z., 2021. An overview of the characteristic of typical Wufeng–Longmaxi shale gas fields in the Sichuan Basin, China. Nat. Gas Ind. B 8, 217–230. https://doi.org/10.1016/j.ngib.2021.04.001.
- Orr, C., 1977. Surface area measurement. In: Treatise on Analytical Chemistry: Part III. Analytical Chemistry in Industry. New York, pp. 321–358.
- Pal-Bathija, A., Prasad, M., Liang, H., Upmanyu, M., Lu, N., Batzle, M., 2008. Elastic properties of clay minerals. In: SEG Technical Program Expanded Abstracts 2008.
 Presented at the SEG Technical Program Expanded Abstracts 2008. Society of Exploration Geophysicists, pp. 1610–1614. https://doi.org/10.1190/1.3059217.
 Passey, Q.R., Bohacs, K.M., Esch, W.L., Klimentidis, R., Sinha, S., 2010. From oil-prone
- Passey, Q.R., Bohacs, K.M., Esch, W.L., Klimentidis, R., Sinha, S., 2010. From oil-prone source rock to gas-producing shale reservoir geologic and petrophysical characterization of unconventional shale-gas reservoirs. In: All Days. Presented at the International Oil and Gas Conference and Exhibition in China. SPE, Beijing, China. https://doi.org/10.2118/131350-MS p. SPE-131350-MS.
- Peltonen, C., Marcussen, Ø., Bjørlykke, K., Jahren, J., 2009. Clay mineral diagenesis and quartz cementation in mudstones: the effects of smectite to illite reaction on rock properties. Mar. Pet. Geol. 26, 887–898. https://doi.org/10.1016/j. marpeteeo.2008.01.021.
- Petersen, H.I., Schovsbo, N.H., Nielsen, A.T., 2013. Reflectance measurements of zooclasts and solid bitumen in lower Paleozoic shales, southern Scandinavia: correlation to vitrinite reflectance. Int. J. Coal Geol. 114, 1–18. https://doi.org/ 10.1016/j.coal.2013.03.013.
- Podhalańska, T., 2009. The late Ordovician Gondwana glaciation– a record of environmental changes in the depositional succession of the Baltic Depression (Northern Poland). (in Polish with English summary). Pr. Państwowego Inst. Geol.
- Poprawa, P., 2010. Potencjał występowania złóż gazu ziemnego w łupkach dolnego paleozoiku w basenie bałtyckim i lubelsko-podlaskim. Prz. Geol. 58, 226–249
- Poprawa, P., Šliaupa, S., Stephenson, R., Lazauskien, J., 1999. Late Vendian–Early Palæozoic tectonic evolution of the Baltic Basin: regional tectonic implications from subsidence analysis. Tectonophysics 314, 219–239. https://doi.org/10.1016/S0040-1951(99)00245-0.
- Porębski, S.J., Prugar, W., Zacharski, J., 2013. Silurian shales of the east European Platform in Poland-some exploration problems. Prz. Geol. 61, 630–638.
- Prasad, M., Kopycinska, M., Rabe, U., Arnold, W., 2002. Measurement of Young's modulus of clay minerals using atomic force acoustic microscopy. Geophys. Res. Lett. 29. https://doi.org/10.1029/2001GL014054.
- Ross, D.J.K., Bustin, R.M., 2009. The importance of shale composition and pore structure upon gas storage potential of shale gas reservoirs. Mar. Pet. Geol. 26, 916–927. https://doi.org/10.1016/j.marpetgeo.2008.06.004.
- Rouquerol, J., Avnir, D., Fairbridge, C.W., Everett, D.H., Haynes, J.M., Pernicone, N., Ramsay, J.D.F., Sing, K.S.W., Unger, K.K., 1994. Recommendations for the characterization of porous solids (technical report). Pure Appl. Chem. 66, 1739–1758. https://doi.org/10.1351/pac199466081739.
- Sahoo, A.K., Mukherjee, D., Mukherjee, A., Srivastava, M., 2013. Reservoir characterization of Eagle Ford Shale through lithofacies analysis for identification of sweet spot and best landing point. In: Unconventional Resources Technology Conference, Denver, Colorado, 12–14 August 2013. Presented at the Unconventional

- Resources Technology Conference. Society of Exploration Geophysicists, American Association of Petroleum Geologists, Society of Petroleum Engineers, Denver, Colorado, USA, pp. 1376–1383. https://doi.org/10.1190/urtec2013-139.
- Sandvik, E.I., Young, W.A., Curry, D.J., 1992. Expulsion from hydrocarbon sources: the role of organic absorption. Org. Geochem. 19, 77–87. https://doi.org/10.1016/ 0146-6380(92)90028-V.
- Schieber, J., 2010. Common themes in the formation and preservation of intrinsic porosity in shales and mudstones illustrated with examples across the phanerozoic. In: All Days. Presented at the SPE Unconventional Gas Conference. SPE, Pittsburgh, Pennsylvania, USA. https://doi.org/10.2118/132370-MS p. SPE-132370-MS.
- Schieber, J., Lazar, R., Bohacs, K., Klimentidis, R., Dumitrescu, M., Ottmann, J., 2016. An SEM study of porosity in the Eagle Ford Shale of Texas—pore types and porosity distribution in a depositional and sequence-stratigraphic context. In: Breyer, J. (Ed.), The Eagle Ford Shale. American Association of Petroleum Geologists, pp. 167–186. https://doi.org/10.1306/13541961M1103589.
- Schoenherr, J., Littke, R., Urai, J.L., Kukla, P.A., Rawahi, Z., 2007. Polyphase thermal evolution in the Infra-Cambrian Ara Group (South Oman Salt Basin) as deduced by maturity of solid reservoir bitumen. Org. Geochem. 38, 1293–1318. https://doi.org/ 10.1016/j.orggeochem.2007.03.010.
- Skret, U., Fabianska, M.J., 2009. Geochemical characteristics of organic matter in the lower Palaeozoic rocks of the Peribaltic Syneclise (Poland). Geochem. J. 43, 343–369. https://doi.org/10.2343/geochemj.1.0034.
- Stomski, P., Szczepański, J., Topór, T., Mastalerz, M., Pluymakers, A., Derkowski, A., Wojciechowski, T., 2021. Factors controlling pore network development of thermally mature early Palaeozoic mudstones from the Baltic Basin (N Poland). Mar. Pet. Geol. 134, 105328. https://doi.org/10.1016/j.marpetgeo.2021.105328.
- Stankiewicz, A., Ionkina, N., Motherwell, B., Bennett, B., Wint, O., Mastalerz, M., 2015. Kerogen density revisited—lessons from the Duvernay shale. In: Proceedings of the 3rd Unconventional Resources Technology Conference. Presented at the Unconventional Resources Technology Conference. American Association of Petroleum Geologists, San Antonio, Texas, USA. https://doi.org/10.15530/urtec-2015-2157904.
- Strapoć, D., Mastalerz, M., Schimmelmann, A., Drobniak, A., Hasenmueller, N.R., 2010. Geochemical constraints on the origin and volume of gas in the New Albany Shale (Devonian–Mississippian), eastern Illinois Basin. Bulletin 94, 1713–1740. https://doi.org/10.1306/06301009197.
- Suárez-Ruiz, I., Juliao, T., Suárez-García, F., Marquez, R., Ruiz, B., 2016. Porosity development and the influence of pore size on the CH4 adsorption capacity of a shale oil reservoir (Upper Cretaceous) from Colombia. Role of solid bitumen. Int. J. Coal Geol. 159, 1–17. https://doi.org/10.1016/j.coal.2016.03.020.
- Teng, J., Liu, B., Mastalerz, M., Schieber, J., 2022. Origin of organic matter and organic pores in the overmature Ordovician-Silurian Wufeng-Longmaxi Shale of the Sichuan Basin, China. Int. J. Coal Geol. 253, 103970. https://doi.org/10.1016/j.coal.2022.103970.
- Topór, T., Derkowski, A., Kuila, U., Fischer, T.B., McCarty, D.K., 2016. Dual liquid porosimetry: a porosity measurement technique for oil- and gas-bearing shales. Fuel 183, 537–549. https://doi.org/10.1016/j.fuel.2016.06.102.
- Topór, T., Derkowski, A., Ziemiański, P., Marynowski, L., McCarty, D.K., 2017a. Multi-variable constraints of gas exploration potential in the lower Silurian shale of the Baltic Basin (Poland). Int. J. Coal Geol. 179, 45–59. https://doi.org/10.1016/j.coal.2017.05.001
- Topór, T., Derkowski, A., Ziemiański, P., Szczurowski, J., McCarty, D.K., 2017b. The effect of organic matter maturation and porosity evolution on methane storage potential in the Baltic Basin (Poland) shale-gas reservoir. Int. J. Coal Geol. 180, 46–56. https://doi.org/10.1016/j.coal.2017.07.005.
- Valenza, J.J., Drenzek, N., Marques, F., Pagels, M., Mastalerz, M., 2013. Geochemical controls on shale microstructure. Geology 41, 611–614. https://doi.org/10.1130/ G33639 1
- Wang, Q., Wang, T., Liu, W., Zhang, J., Feng, Q., Lu, H., Peng, P., 2019. Relationships among composition, porosity and permeability of Longmaxi Shale reservoir in the Weiyuan Block, Sichuan Basin, China. Mar. Pet. Geol. 102, 33–47. https://doi.org/ 10.1016/j.marpetgeo.2018.12.026.
- Wang, J., Liu, Y., Yang, C., Jiang, W., Li, Y., Xiong, Y., Peng, P., 2022. Evolution of mechanical properties of kerogen with thermal maturity. Mar. Pet. Geol. 145, 105006. https://doi.org/10.1016/j.marnetgep.2022.105006
- 105906. https://doi.org/10.1016/j.marpetgeo.2022.105906.
 Wang, D., Li, X., Li, S., Li, G., Mao, T., Zheng, B., 2024. Evolution of pore structure and methane adsorption in lower Silurian Longmaxi Shale: implications for uplifted shale gas reservoirs. Rock Mech. Rock. Eng. 57, 5335–5353. https://doi.org/10.1007/s00603-023-03441-w.
- Wei, L., Mastalerz, M., Schimmelmann, A., Chen, Y., 2014. Influence of Soxhlet-extractable bitumen and oil on porosity in thermally maturing organic-rich shales. Int. J. Coal Geol. 132, 38–50. https://doi.org/10.1016/j.coal.2014.08.003.
- Wood, J.M., Sanei, H., Curtis, M.E., Clarkson, C.R., 2015. Solid bitumen as a determinant of reservoir quality in an unconventional tight gas siltstone play. Int. J. Coal Geol. 150–151, 287–295. https://doi.org/10.1016/j.coal.2015.03.015.
- Wood, J.M., Sanei, H., Haeri-Ardakani, O., Curtis, M.E., Akai, T., Currie, C., 2018. Solid bitumen in the Montney Formation: diagnostic petrographic characteristics and significance for hydrocarbon migration. Int. J. Coal Geol. 198, 48–62. https://doi. org/10.1016/j.coal.2018.09.004.
- Xu, C., Yao, S., Song, D., Liu, Y., 2020. Types, chemical and porosity characteristics of hydrocarbon-generating organisms of the lower Paleozoic, South China—taking Longmaxi Formation and Qiongzhusi Formation in Sichuan Basin as examples. Mar. Pet. Geol. 119, 104508. https://doi.org/10.1016/j.marpetgeo.2020.104508.
- Yuan, W., Liu, M., Chen, D., Xing, Y.-W., Spicer, R.A., Chen, J., Them, T.R., Wang, X., Li, S., Guo, C., Zhang, G., Zhang, L., Zhang, H., Feng, X., 2023. Mercury isotopes

show vascular plants had colonized land extensively by the early Silurian. Sci. Adv.

9, eade9510. https://doi.org/10.1126/sciadv.ade9510.
Zhang, W., Hu, W., Borjigin, T., Zhu, F., 2020. Pore characteristics of different organic matter in black shale: a case study of the Wufeng-Longmaxi Formation in the

Southeast Sichuan Basin, China. Mar. Pet. Geol. 111, 33–43. https://doi.org/ 10.1016/j.marpetgeo.2019.08.010.
Ziegler, P.A., 1990. Geological Atlas of Western and Central Europe.